



Stockholm
University

Master Thesis

Degree Project in
Geology 45 hp

Defining the geochemical footprint for gold mineralisation around Birthday Reef. Reefton Goldfield, New Zealand

Jonathan Hamisi



Stockholm 2016

Department of Geological Sciences
Stockholm University
SE-106 91 Stockholm
Sweden

**Defining the geochemical footprint for gold mineralisation around Birthday Reef.
Reefton Goldfield, New Zealand**

Jonathan Hamisi

Degree project in Geology 45hp

Credit front page picture

Photographer: Joseph Divis, Derek French collection (West Coast Historical Museum)
'Working underground at Blackwater Mine', URL: <http://www.nzhistory.net.nz/media/photo/working-underground-blackwater-mine>, (Ministry for Culture and Heritage), updated 15-Jul-2013

Contents

LIST OF SULFIDES MINERAL FORMULA.....	3
LIST OF FIGURES AND TABLES	4
ABSTRACT	5
1. INTRODUCTION.....	6
2. GEOLOGICAL SETTING.....	8
2A. NEW ZEALAND.....	8
2B. OROGENIC GOLD DEPOSIT IN NEW ZEALAND	9
2C. REEFTON AREA.....	12
2D. REEFTON GOLD DEPOSITS	12
3. OROGENIC GOLD DEPOSITS.....	13
3A. GENERAL CHARACTERISTICS.....	13
3C. ORE FORMING SYSTEM - SOURCE TO SINK	16
3D. ALTERATION - PROXIMAL AND DISTAL	17
4. SAMPLING	18
5. ANALYTICAL METHODS.....	19
XRF/LA-ICPMS	19
ULTRALOW DETECTION LIMIT ANALYSIS FOR AU, AS AND SB	20
IN-SITU LA-ICPMS.....	20
SEM AND MICROSCOPY	20
6. RESULTS	21
6A. LITHOGEOCHEMISTRY	21
6B. MINERALOGY.....	27
<i>Wall rock alteration</i>	27
Protolith	27
Distal alteration zone.....	28
Proximal alteration zone.....	29
<i>Ore zone alteration</i>	31
<i>Mineral paragenesis synthesis</i>	32
6C. IN-SITU MINERAL CHEMISTRY	32
<i>Distribution of Au, As and Sb in sulfides</i>	32
<i>Other trace elements</i>	34
7. DISCUSSION	36
7A. PROTOLITH COMPOSITION.....	36
7B. MASS BALANCE	38
<i>Gold (Au)</i>	38
Distal alteration.....	39
Proximal alteration	39
<i>Arsenic (As)</i>	39
Distal alteration.....	40
Proximal alteration	40
<i>Antimony (Sb)</i>	40
Distal alteration.....	42
Proximal alteration	42
<i>Potassium (K₂O) and sodium (Na₂O)</i>	42
Distal alteration.....	42

Proximal alteration	44
7C. HYDROTHERMAL ALTERATION	44
7D. MINERAL CONTROL ON MASS CHANGE	47
7E. ORE DEPOSIT FOOTPRINT	48
8. CONCLUSIONS	50
9. ELECTRONIC SUPPLEMENTARY MATERIALS (ESM) APPENDIX	51
REFERENCES	52
ACKNOWLEDGEMENTS	57

List of sulfides mineral formula

Name	Abbreviation	Mineral formula
Arsenopyrite	Apy	FeAsS
Electrum		(Au,Ag)
Chalcopyrite	Ccp	CuFeS ₂
Cobaltite	Co	CoAsS
Galena	Gn	PbS
Gersdorffite	Gsdf	NiAsS
Millerite	Mr	NiS
Pentlandite	Pn	(Fe,Ni) ₉ S ₈
Pyrite	Py	FeS
Sphalerite	Sp	(Zn,Fe)S
Tetradymite		Bi ₂ Te ₂ S
Ullmanite	Ullm	NiSbS

List of figures and tables

Fig. 1: Gold trend from 1973 to 2015.	6
Fig. 2: Basement terranes of onshore New Zealand.	9
Fig. 3: A. Location and past gold production in tons (t) of deposits of the Reefton goldfield and other orogenic (mesothermal) gold deposits hosted in Early Palaeozoic metasedimentary rocks of the Buller terrane, South Island, New Zealand. B. Regional geology and location of some of the 84 former gold mines in the Reefton goldfield.	10
Fig. 4: Orogenic gold deposits in Paleozoic and Mesozoic metasediments of South Island, New Zealand. A. West coast and Fjordland. B: Marlborough, Southern Alps and Otago..	11
Fig. 5 : Schematic diagram showing the tectonic setting of various gold deposit types.	14
Fig. 6: A. Schematic architecture of lode gold hydrothermal system from the source to sink and formation of the ore deposit. B. Cordilleran-type orogeny recognised for the widespread distribution of orogenic gold deposits in metamorphosed juvenile rocks on either side of the magmatic arc.....	16
Fig. 7: Schematic summary of the paragenetic alteration sequence around orogenic gold deposits hosted in metasedimentary rocks at greenschist facies..	18
Fig. 8: Sediments classification.....	21
Fig. 9 : Box plot of abundance in Na ₂ O K ₂ O, LOI@550, Au, As, Sb, Cr, Ni, Cu, Zn, Mo, W and Bi in all the 72 samples collected on the drill core W21 and W21c at Blackwater.....	22
Fig. 10 : Concentration of Au, As and Sb downhole.....	25
Fig. 11: Concentration of Na ₂ O, K ₂ O & LOI@550 downhole..	26
Fig. 12: Molar Ca/Ti versus CO ₂ /Ti.	27
Fig. 13: Microscope images in transmitted light (A, E and G), reflected light (B) and SEM Photomicrographs (C, D, F and H).....	30
Fig. 14: Scans of polish thin sections.....	31
Fig. 15: Mineral paragenesis of Blackwater	33
Fig. 16: Trace element abundance in sulfides minerals. Au, As, Sb and Ag.....	34
Fig. 17: Trace element abundance in sulfides minerals. Se, Te and Hg.	35
Fig. 18: Isochon diagrams showing immobile elements and elements that have undergone gain or loss during alteration. A) Argilite. B) Metagraywacke.	37
Fig. 19: Strip log illustrating the % Δ Au mobility in the distal and proximal alteration relative to the unaltered host rock.....	39
Fig. 20: Strip log illustrating the % Δ As mobility in the distal and proximal alteration relative to the unaltered host rock.....	40
Fig. 21: Strip log illustrating the % Δ Sb mobility in the distal and proximal alteration relative to the unaltered host rock.....	42
Fig. 22: Strip log illustrating the K ₂ O (A) and Na ₂ O (B) mobility in the distal and proximal alteration relative to the unaltered host rock.	44
Fig. 23: Profiles showing weighed average of Au, As, Sb and alteration index footprint.	46
Fig. 24: Mineralogical and geochemical footprint of Blackwater Au deposit.....	49

Abstract

Orogenic gold deposits from the Reefton goldfield in New Zealand hosted in Ordovician metasediments of the Greenland group have produced 67 tons of gold before 1951. The Blackwater mine in Waiuta accounts for about 1/3 of the gold production at Reefton prior to 1951. The ore system at Blackwater consists of NE trending steeply dipping gold-bearing quartz veins (Birthday reef) occurring in faulted, sheared and folded alternating sequence of sandstone-mudstone metamorphosed to low greenschist facies and hydrothermally altered proximal to distal from the quartz vein. Host rock and ore forming fluids interaction resulted in a systematic change in the mineralogy and geochemistry of the wallrock developing a distinctive footprint of the ore system. The mineral assemblage subsequent to hydrothermal alteration is formed by quartz veining, chlorite, carbonates (minor calcite-dolomite-ankerite-siderite), albite, K-Mica and composite quartz-carbonate veining, carbonates spotting, pyrite, arsenopyrite, chalcopyrite, cobaltite, galena and in a lesser extent ullmannite, gersdorffite, pentlandite, millerite and sphalerite. Mass balance calculation based on geochemical data obtained by ultra-low detection analysis with a detection limit in part per trillion of Au, As and Sb provide new insight in the geochemical footprint of the ore system at Blackwater. A clear zone of roughly 40 meters (20 meters above and below the birthday reef) is enriched in Au, As and Sb up to respectively 6806%, 605% and 891% compared to the un-mineralised protolith. Furthermore, mass changes in K_2O and Na_2O indicate a consistent decrease in Na and increase in K in the vicinity of the Birthday reef reflecting the replacement of albite by K-mica. This is corroborated by pattern of alkali alteration index Na/Al for albite and $3K/Al$ for K-Mica showing similar trend. Carbonation and de/hydration index also exhibits peaks in samples adjacent to the Birthday reef, though carbonation index is also influenced by carbonates content in the protolith or late carbonation that may not be related to gold mineralisation. Using the indicators above-mentioned it is possible to define the mineralogical and geochemical "footprint" for the ore system in the host rock allowing to use this footprint as a tool for mineral exploration for orogenic gold deposits similar to Blackwater. Given that the geochemical footprint of orogenic gold deposit such as Blackwater is significantly wider than the economically viable part of the deposit defining the footprint of the ore system offers the potential for vectoring from sub-economic mineralisation towards higher-grade ore that is economically viable.

Keywords: *Orogenic gold, hydrothermal alteration, Reefton, mass changes, geochemical footprint, vectors, exploration, Blackwater*

1. Introduction

Orogenic gold deposits are a major source of gold accounting for more than 25% of gold production worldwide, even up to 75% if placer deposits, secondary products of orogenic gold deposits are included (Fu et al. 2007). There has been a significant increase of the gold price in the late 1970s, reaching U.S.\$ 800/oz in January 1980 (Price 2015), and more recently in 2012 reaching almost U.S.\$ 2000/oz (Fig. 1). This increase of gold price is mainly due to growing demand in developing countries such as China, India and Russia, and economic forecasts predict continuous growth in the gold demand. The last decade has seen a significant decline in the number of major gold deposits discovered (>2.5 Moz Au) and in the amount of gold contained in these deposits, compared to the early to mid-1990s (SNL Metals Economics Group 2013). Better understanding of the ore-forming systems is critical for more successful exploration and discovery of new ore deposits. One approach to generate better understanding of the ore forming system and at the same time a practical tool for exploration is to define the geochemical and mineralogical footprint of known gold deposit. The footprint represents the subtle geochemical effects of the hydrothermal ore forming process that occur more distal from the deposit, and as such it can be used to target the ore deposit itself. This thesis aims to define the geochemical footprint of the Blackwater Gold deposit in the Reefton, New Zealand.



Fig. 1 Gold price trend from 1973 to 2015. Source: www.goldprice.org

Orogenic gold deposits form in deformed metamorphic belts at mid-crustal levels and are the product of flow of gold-bearing hydrothermal fluid during orogeny, hence the term 'Orogenic Gold' (Groves et al. 1998). The gold bearing ore bodies which are in general quartz lodes (veins), form in host rocks during the late stage of deformation and metamorphism. The quartz lodes generally form at greenschist facies although some deposits have been reported in sub-greenschist and amphibolite facies rocks (Vielreicher et al. 2002). Orogenic gold deposits have formed throughout the Earth's history, intermittently from the Middle Archean to younger Precambrian, and continuously through the Phanerozoic. The production and resources from economic Phanerozoic orogenic-gold deposits are estimated at about one billion ounces of gold. Orogenic gold deposits commonly occur in regionally metamorphosed terranes and they form during compressional to transpressional deformation processes at convergent plate margins in accretionary and collisional orogeny (Groves et al. 1998). The deposits are spatially associated with steeply-dipping transcrustal fault systems that are parallel to the strike of the orogeny (Cox 2005). Orogenic gold deposits are generally associated with gold rich placers accumulations.

The flow of gold bearing hydrothermal fluids forming the gold deposit results in anomalous and systematic mineralogical and geochemical changes of the surrounding host rock (Eilu et al. 2001).

The new mineral assemblages and the geochemical trends resulting from the fluid and host rock interaction forms the geochemical “footprint” of the ore system that is targeted in gold exploration at regional or deposit scale. The geochemical footprint can, in some cases, be mapped for several hundred meters far beyond the economically viable portion of the deposit by means of some ‘pathfinders’ elements. The geochemical halo associated with orogenic gold deposits can be defined by variable degree of enrichment/depletion of Au and other “pathfinders” elements including As, Hg, Mo, Sb, Se, Te, Ag and W. The mineralogical halo involves replacement of metamorphic minerals by hydrothermal minerals through sulphidation, carbonation, sericitisation, and chloritisation, (Christie & Brathwaite 2003). Hence, if well constrained, the ore deposit footprint offer the potential to vector from low-grade sub-economic mineralisation towards higher-grade ore.

Three main ages of orogenic gold deposit occur in New Zealand; Palaeozoic deposits that occur west of the Alpine Fault, Mesozoic deposits that occur in the Otago Schists, and Miocene to recent deposits that occur in the Southern Alps. In this study, I investigate the mineral paragenesis and geochemical signature along a 1.65km drill core from a Palaeozoic goldfield near Reefton west of the Alpine Fault. The drill core was recovered from Waiuta during the exploration programme carried out by Oceana Gold Corporation at the Blackwater Mine in the southern part of the Reefton. The drilling intersected an orogenic gold system formed by steeply dipping shear zones hosting gold-bearing quartz lodes in Cambro-Ordovician metasedimentary rocks of the Greenland Group (Christie & Brathwaite 2003). A suite of 72 samples were collected from the Blackwater drill core WA21 & WA21C. The drill core sampled over 1.5km of unmineralised host rock of relatively consistent lithologies (alternating sandstone and mudstone) distal to proximal from the gold bearing veins as well as the quartz lodes itself referred to as “Birthday reef”. As such, it provides a unique opportunity to investigate the distal to proximal mineralogical and geochemical changes that occurred during hydrothermal alteration. The distal to proximal variation in the mineralogy and the rocks chemistry forms the geochemical “footprint” of the orogenic ore system at Reefton.

The footprint can be used as a gradient for vectoring towards the ore deposit during mineral exploration going from sub-economic very low-grade rocks toward economic and viable high-grade and gold rich rocks. Geochemical analysis of drill core samples including ultralow detection limit analysis for Au, As & Sb were used to investigate element mobility and quantify enrichments and/or depletions of these elements in order to constrain the distal to proximal ore system footprint. Samples were also analysed for their abundance in major oxides and trace elements in order to investigate the geochemical variation between the metasedimentary protolith rocks and the hydrothermally altered rocks adjacent to the quartz lodes. Mineralogical investigations were conducted by means of microscopy and scanning electron microscope (SEM) in order to identify the paragenetic sequence of mineralisation and the more subtle mineral changes that occur distal from the deposit. The in-situ *Laser Ablation Inductively Coupled Plasma Mass Spectrometry* (LA-ICPMS) analysis of sulfides minerals enabled constraint of the host minerals for gold in the hydrothermal alteration halo.

2. Geological Setting

2a. New Zealand

The New Zealand crustal block is a fragment of the supercontinent Gondwana located to the southwest of the Pacific Ocean. Before Late Cretaceous sea floor spreading it was contiguous with Australia and Antarctica. New Zealand lies astride a zone of collisional plate boundary - Pacific and Australian plates - with current oblique convergence occurring at 38mm/year and is part of the Pacific Ring of Fire (Fig. 2). New Zealand extends over a large area mainly submerged (>85%), 2 distinct islands - North & South Islands - of the continent are emerged above the sea level (Sutherland 1999). The South Island, where the Reefton area is located, is composed by tectonostratigraphic terranes and igneous suites (Coombs et al. 1976; Bishop et al 1985; Bradshaw 1989; Mortimer&Tulloch 1996), which were accreted to the margin of the supercontinent Gondwana during late Palaeozoic and Mesozoic time.

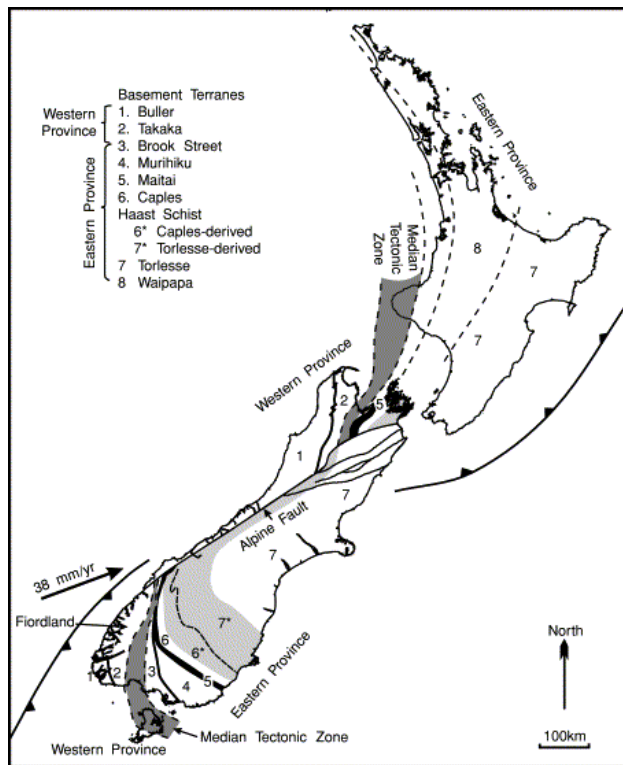
The Western region of the South Island is composed mainly of Late Cambrian–Ordovician greywacke metasediments that form the Buller Terrane. These sedimentary rocks are regionally metamorphosed and locally intruded by Palaeozoic granitoids (Nathan 1976; Tulloch 1983; Tulloch 1988; Cooper and Tulloch 1992). The Takaka Terrane is smaller volumetrically and is composed of a diverse assemblage of deformed and metamorphosed Palaeozoic sedimentary and volcanic rocks (Bishop et al 1985; Cooper & Tulloch 1992).

The Eastern region consist of lithic and feldspathic metagraywacke, but also include volcanic, intrusive, and ophiolitic assemblages (Coombs et al. 1976; MacKinnon 1983; Bishop et al. 1985; Kimbrough et al. 1992; Balance & Campbell 1993; Roser et al. 1993; Mortimer 1995). The Haast Schist separates weakly metamorphosed Caples and Torlesse terrane sediments, and represents a metamorphic overprint on at least these two terranes (Adams & Gabites 1985; Graham & Mortimer 1992).

The Median Tectonic Zone (Landis & Coombs 1967) separates Western Province from Eastern Province rocks, and consists of a suite of subduction-related calc-alkaline plutons with subordinate volcanic and sedimentary rocks (Bradshaw 1993; Kimbrough et al 1994). Magmatic ages range from Carboniferous to Early Cretaceous, with apparent gaps in the Permian and Middle Jurassic (Kimbrough et al. 1994; Bradshaw et al. 1997). Carboniferous rocks are rare in the Median Tectonic Zone and their significance is still unclear (Kimbrough et al. 1994).

The present shape of the New Zealand continent is mainly the result of Cretaceous–Cenozoic tectonics. During the period 130–80 Ma, there was a change from subduction-related processes to extension and widespread basin formation (Bradshaw 1989), eventually ending in seafloor spreading and formation of the Tasman Sea and South Pacific. During Late Cretaceous–Late Eocene time, the New Zealand continent had a passive margin setting and was relatively calm tectonically. A new plate boundary propagated through New Zealand at ~45 Ma. Between 45 and 30 Ma, the instantaneous pole of Australia–Pacific rotation was near New Zealand (Sutherland 1995). Cenozoic strike-slip

faulting overprints earlier deformation, and is most clearly manifested by a 460 km apparent offset of the Maitai Terrane by the Alpine Fault (Clark & Wellman 1959).



The Alpine Fault is the main active structure in the oblique continental collision zone of the South Island. It is continuous at the surface for ~800 km and accommodates ~70% of current plate motion (Sutherland et al. 2000). The total Eocene–Recent plate motion through South Island is well constrained as ~850 km (Sutherland 1995). No Precambrian cratonic core is exposed “onland” in New Zealand (Sutherland 1999).

Fig. 2: Basement terranes of onshore New Zealand (Sutherland 1999) after Bishop et al. (1985), Kimbrough et al. (1994), Mortimer (1995), and Mortimer et al. (1997).

2b. Orogenic gold deposit in New Zealand

Orogenic gold deposits in New Zealand can be classified in 3 groups according to their age of formation: Paleozoic, Mesozoic and Miocene to recent. Paleozoic orogenic gold deposits are essentially hosted in late Cambrian-Ordovician sequence of alternating metagraywacke (sandstone/siltstone) and meta-argillite (mudstone) of the Greenland group (Fig. 3 and Fig. 4A). The gold-bearing lodes are made of lensoid quartz shoot developed along shear zones that dip steeply and usually strike parallel to the axes of folding in the host rocks, even though some are discordant and cut through the bedding (Christie & Brathwaite 2002). The visible mineralogical halo resulting from host rock alteration consists of arsenopyrite, pyrite, carbonates, chlorite and sericite. This halo is a few centimeters to meters wide in the host rock adjacent to the quartz lodes (Christie & Brathwaite 2003).

The deposits in Paleozoic metasediments include the ones at Golden Blocks (~1,11T Au) in Northwest Nelson, Lyell (2,84T Au) and Reefton (67T Au) on the West Coast, and Preservation Inlet (0,28T Au) in Fjordland. The Reefton Goldfield contains the most significant orogenic gold deposits on the West Coast of the South Island in New Zealand (GNS 2012). More than 67 tons of gold were produced from these deposits including 84 mines between 1870 and 1951.

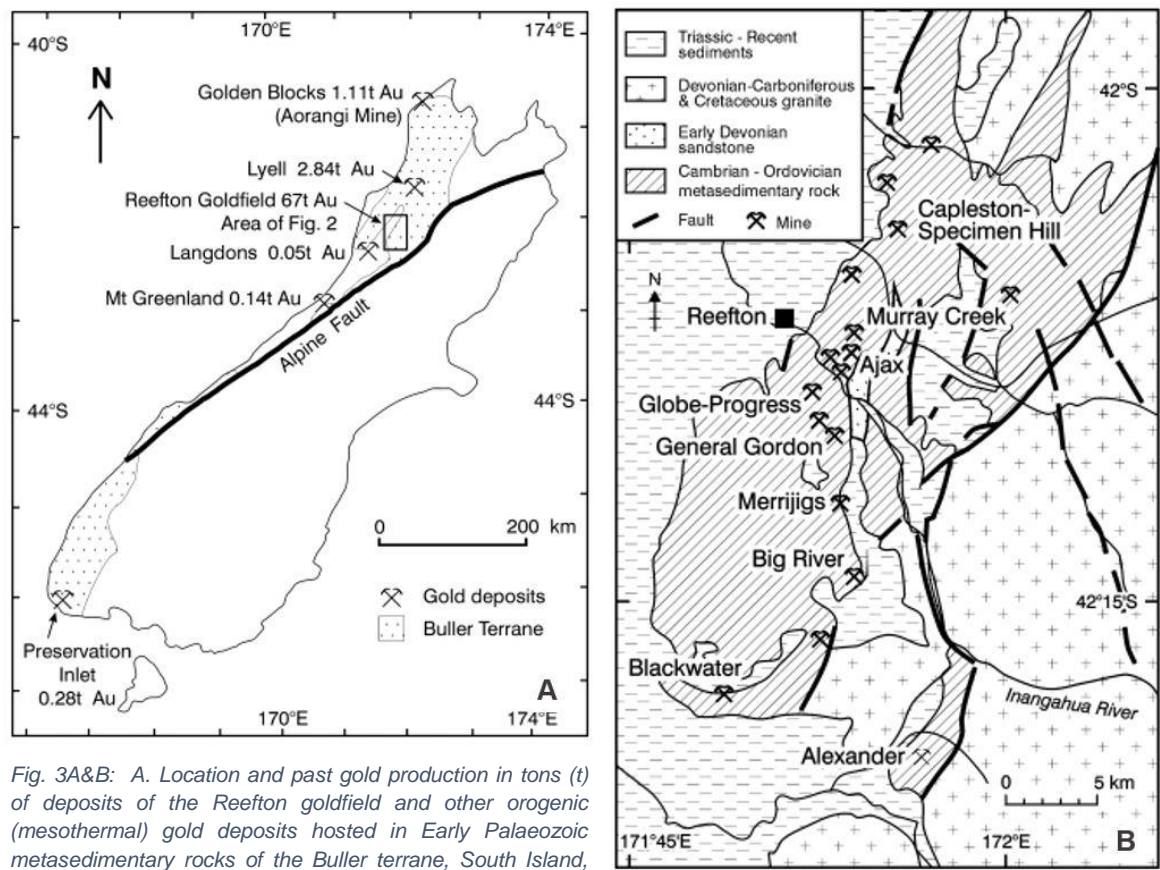


Fig. 3A&B: A. Location and past gold production in tons (t) of deposits of the Reefton goldfield and other orogenic (mesothermal) gold deposits hosted in Early Palaeozoic metasedimentary rocks of the Buller terrane, South Island, New Zealand. B. Regional geology and location of some of the 84 former gold mines in the Reefton goldfield.

The gold-bearing quartz lodes are hosted within a NNE-trending belt, having around 34 km in length and 10 km in width. The metasedimentary rocks consist of alternating sandstone and mudstone beds that were metamorphosed to lower greenschist facies prior being hydrothermally altered with the metamorphic mineral assemblage of quartz, albite, muscovite and chlorite (Christie & Brathwaite 2003). The largest known deposits were worked at the Blackwater and Globe-Progress mines.

At the Blackwater Mine, the Birthday reef averaged less than one metre in width but had a strike length of 1070 meters and was mined down to a depth of 830 meters, to produce 23t of gold between 1909 and 1951. Quartz lodes at the Globe Progress mine produced 13t of gold between 1879 and 1920. Most of the deposit at Reefton are formed by mineralised quartz lodes but deposit such Globe-Progress contains a significant disseminated mineralisation and show a development of a larger hydrothermal alteration halo. Blackwater and Globe-Progress are currently being further explored.

The Paleozoic orogenic gold deposits in New Zealand show many resemblances to the Bendigo-Ballarat deposits in Victoria, Australia (Ramsay et al. 1998; Bierlein et al. 2004). In some of the Victorian deposits there is a notable phase of gold mineralisation that is Sb-rich and superimposed on pre-existing gold-bearing quartz veins at a substantially later time (Bierlein et al. 2004; Bierlein & Maher 2001) Both Victoria and Reefton goldfields developed in the Early Palaeozoic as a result of accretionary processes along the active continental margins of Gondwana (Bierlein et al. 2004).

The Reefton goldfield represent a perfect natural laboratory to define the footprint of orogenic gold systems because the gold-bearing quartz lodes are hosted in a relatively homogenous succession of metagraywacke and argillite allowing to compare protolith background variation with hydrothermally altered rocks of having fairly the same composition.

The Mesozoic orogenic gold deposits (Fig. 4B) are hosted in schist of Otago and Marlborough, and schist and greywacke of the Southern Alps (Christie & Brathwaite 2003). Historically, the Mesozoic deposits were mined from underground mining of very narrow steeply dipping quartz lodes and had a fairly low gold production (GNS 2012). However, 2 decades ago, the Macraes mine, currently the largest gold mine in New Zealand was discovered in the Mesozoic schist. The deposit is hosted in a shallow dipping shear zone and represent the major Mesozoic deposit in the South Island. The hydrothermal minerals consist essentially of quartz and illite and extend only a few centimeters adjacent to the quartz lodes. The common sulfides in the Mesozoic deposits are Pyrite and Arsenopyrite but accessorily chalcopyrite, sphalerite, cinnabar and galena are present.

Some of the Mesozoic deposits show anomalous enrichment in other orogenic gold-related elements including W and Sb. Scheelite (CaWO_4) was mined from lodes at Wakamarina, Glenorchy, Macraes and Barewood and is it present in many other Mesozoic deposits. Stibnite (Sb_2S_3) was mined at Endeavour Inlet and Carrick, but is also present at Macetown, Hidon, Waipori and Nenthon (Christie & Brathwaite 2003).

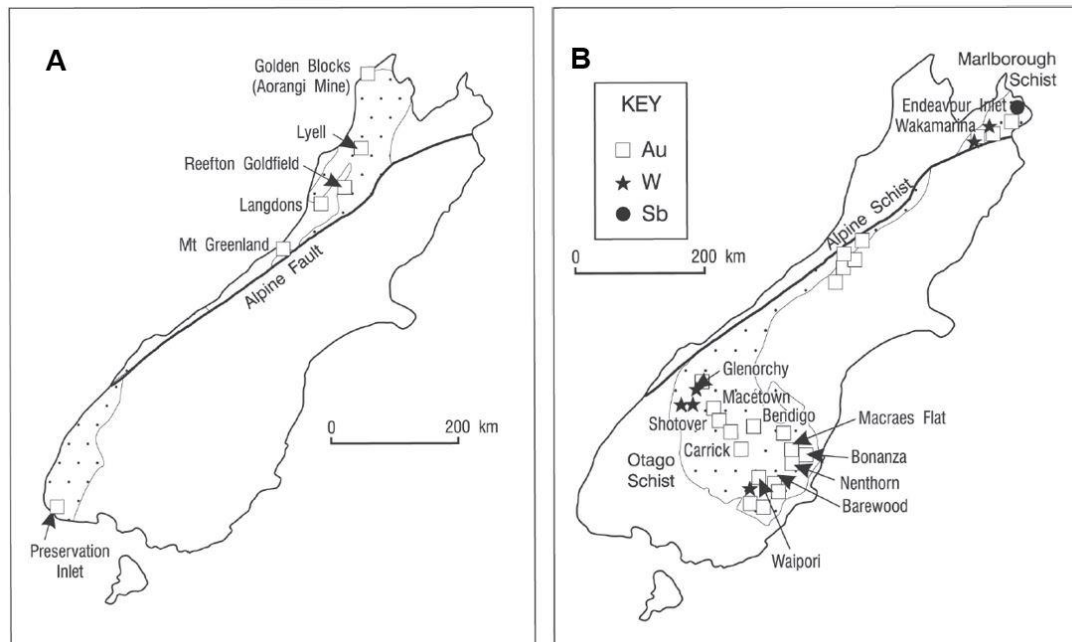


Fig. 4A&B: Orogenic gold deposits in Paleozoic and Mesozoic metasediments of South Island, New Zealand. A. West coast and Fjordland. B. Marlborough, Southern Alps and Otago. After Christie & Brathwaite 2003.

Miocene to recent gold-bearing quartz lodes in the Southern Alps are hosted by the Haast schist, the greywacke of the Taipo river and metagreywacke of the Wilberforce river (Williams 1974a). However no significant gold production was recorded from these quartz lodes. They have been associated with the Mesozoic deposit of the Otago schist but Marlborough structural features may suggest a Cenozoic

age and probably relate to the late Cenozoic deformation associated with rapid uplift along the Alpine fault (Craw et al. 1987; Becker et al. 2000). Erosion of both Palaeozoic and Mesozoic deposits in New Zealand resulted in formation of large placers deposits from Miocene to recent for the Palaeozoic deposits and from Cretaceous to recent for the Mesozoic deposits in the Otago schist.

2c. Reefton Area

The Reefton area consist of a 34 km by 10 km belt of Cambrian–Ordovician metasedimentary rocks of the Buller terrane (Fig. 3B) having a NNE-trend (Christie & Brathwaite 2003). These metasedimentary rocks are classified as Greenland Group (Cooper 1974; Adams et al. 1975; Nathan 1978; Adams & Kelley 1998). The Greenland Group consists of an alternating sequences of indurated sandstone and mudstone turbidites resulting from weathering of a passive continental margin (Roser et al. 1996). The rock sequence is strongly folded and regionally metamorphosed to lower greenschist facies in the Reefton area (Roser & Nathan 1997). Adams et al. (1975) estimated that metamorphism was Silurian to Devonian, based on K–Ar dates of 438 to 395 Ma.

The belt of Greenland Group rocks is bordered on its eastern and northern sides by plutons of the Karamea Batholith (Devonian–Carboniferous and Cretaceous granite in Fig. 3B). Some localities have been affected by contact metamorphism with presence of hornfels and development of albite, epidote and biotite. Mafic dykes have also intruded locally the Greenland Group. Some are pre-mineral and contain gold-bearing quartz lodes, such as in the former Inglewood mine (Fig. 3B) of the Ajax Group (Downey 1928), whereas others are post-mineral, such as the Middle Jurassic Kirwans Dolerite (Mortimer 1995) and a suite of Early Cretaceous lamprophyre dikes. Henderson (1917) reported mafic dikes from several of the gold mining areas including Murray Creek, Ajax and Blackwater (Waiuta). Early Devonian, Triassic, Cretaceous and Tertiary sedimentary rocks forms the fault-bounded blocks within rocks of the Greenland Group.

The Greenland Group belt is bordered to the west by Tertiary sediments, and Late Pliocene–Quaternary fluvio-glacial and alluvial gravels. To the south, the belt passes under Quaternary gravels.

2d. Reefton gold deposits

The Reefton goldfield shows many of the classic characteristics of orogenic gold deposits (Goldfarb et al. 2005). Regional structural mapping by Rattenbury & Stewart (2000) indicated that most of the gold-bearing quartz lodes are limited to a NNE-trending corridor (Fig. 3B) about 5 km in width that compared to the surrounding areas has tighter folds and shorter wavelength. The gold-bearing lodes in the Reefton goldfield are formed by a series of lensoid quartz shoots developed along shear zones that mostly dip steeply and strike N to NNE. According to Christie & Brathwaite (2003) the ore shoots in the deposits range in width from 0.6 to 3.2 metres. Their horizontal extent is very restricted, commonly less than 150 m (1,070 m at Blackwater), but they generally continue down to considerable depth (more than 1,200 m at Blackwater). Ribbon banded, crack-seal textures, defined mainly by phyllosilicate laminae, are characteristic of the veins. Other gangue minerals include carbonates, sericite and chlorite (Christie & Brathwaite 2003).

The gold occurs both as free grains and in association with arsenopyrite and pyrite which are ubiquitous. Stibnite is common in some lodes and in minor amount in others. Minerals that occur in trace quantities include chalcopyrite, galena, sphalerite and the sulphosalts bournonite (PbCuSbS₃), zinkenite (PbSb₂S₄) and tetrahedrite/tennantite (Williams 1974b; Leach et al. 1997). Disseminated gold–arsenopyrite–pyrite–(stibnite) mineralisation occurs between and adjacent to the quartz shoots in several deposits and appears to be best developed at the Globe-Progress deposit (Lew & Corner 1988; Christie et al. 2000).

There are 2 types of mineralisation. The first type is disseminations in poorly veined, non-brecciated sandstone and siltstone. The second is clay-rich fault breccias in the hanging wall and footwall of the lodes (Christie & Brathwaite 2003). The breccias consist of quartz vein and wall rock fragments in a matrix of finely milled vein and wall rock material. Christie & Brathwaite (2003) shows that this brecciation post-dates the main stage of hydrothermal mineralisation that deposited the quartz lodes, and its latest clay-rich phase may be associated with Cretaceous or Tertiary tectonism.

The relative distribution of the disseminated mineralisation and quartz lodes suggests that there are two end member styles of gold deposits in the Reefton goldfield: Globe-Progress has multiple shear zones, quartz lodes and abundant disseminated mineralisation, whereas Blackwater has essentially one major quartz lode, the Birthday reef, with little or no disseminated mineralisation. Christie & Brathwaite (2003) suggested that these differences in style of mineralisation between the Globe-Progress and Blackwater deposits may be partly related to the deformation history. Based on structural study of the deposits in the General Gordon–Merrijigs area (Fig. 3B), Maw (2001) reported that these two deposits and the nearby Globe-Progress deposit were localised at bends or kinks in the surface of the host axial plane shears. In contrast, the Blackwater deposit which is confined to an axial plane shear that has not been subjected to the later kink folding.

The origin and age of the hydrothermal mineralisation in the Reefton goldfield is still debated. One hypothesis (Brathwaite & Pirajno 1993) is that the mineralisation occurred during late stages of folding and thrust faulting associated with Palaeozoic regional metamorphism. This is supported by a K–Ar date of 438 Ma for hydrothermal sericite from Globe-Progress (Hunt & Roddick 1993). An alternative view advanced by Leach et al. (1997) is that the mineralisation is magmatic-related, associated to co-genetic melts associated with post-Jurassic mafic dikes, or to late Early Cretaceous (129–110 Ma) I and I-S type intrusions of the Karamea Batholith.

3. Orogenic gold deposits

3a. General characteristics

Consistent characteristics recognised in orogenic gold deposits include: 1) Deformed and variably altered host rock; 2) Late metamorphic timing, 3) changing far-field stresses in a dominantly subduction/active margin setting, 4) structurally hosted in metamorphosed fore-arc or back-arc setting, 5) a broad thermal equilibrium with host rocks, as indicated by alteration assemblages and lack of zonation, 6) hydrothermal enrichment of K, CO₂, Au, As, Sb, Te, and/or W, 7) low base-metal

contents, and 8) mostly similar over-pressured H₂O-CO₂-CH₄-N₂-H₂S ore fluids specie that commonly go through phase separation (Groves et al. 1998).

Orogenic gold deposits have formed for more than 3Ga during the Earth history. They have formed periodically during from middle Archean to young Precambrian and continuously through the Phanerozoic and are found in three different temporal/tectonic settings (Goldfarb et al. 2001).

The 1st group consist of ores deposits hosted in Late Archean granite-greenstone belts and that were formed between 2750 and 2520 Ma (Saunders et al. 2013). This group of deposits includes amongst others those of the Yilgarn craton (Western Australia), Superior province (Canada), Tanzania craton (central Africa), and Zimbabwe–Kapaal craton (southern Africa). The 2nd group of deposits formed between 2100 and 1730 Ma are hosted in Paleoproterozoic metasedimentary and metavolcanic rocks occurring on the margins of granitoid–greenstone terranes. Favourable host lithologies include banded iron formation and ferruginous chert. The orogenic gold deposits of western Africa, northern South America, and Homestake (USA) are amongst the ones hosted in Paleoproterozoic terranes (Saunders et al. 2013; Goldfarb et al. 2001).

Our study focuses on the 3rd group of orogenic gold deposits formed between 650 and 50 Ma in metamorphosed marine sedimentary rocks adjacent to active continental margins. These deposits includes late Neoproterozoic-Paleozoic gold deposits along the margin of the Gondwana and Laurentia (Pan African Orogeny, Tasman orogeny, Central Asia orogenic belt, etc.) and the Mesozoic to Tertiary gold deposits of the North American Cordilleran orogeny, Colombian Andes, eastern Russia, and the Otago area in New Zealand. The processes forming orogenic gold deposits is continuing today such as at the oblique convergence related to the Alpine fault in New Zealand (Pitcairn et al. 2006), however the absence of significant ore systems younger than 50 Ma reflects the lack of required time for uplift and unroofing of ores formed typically at midcrustal levels.

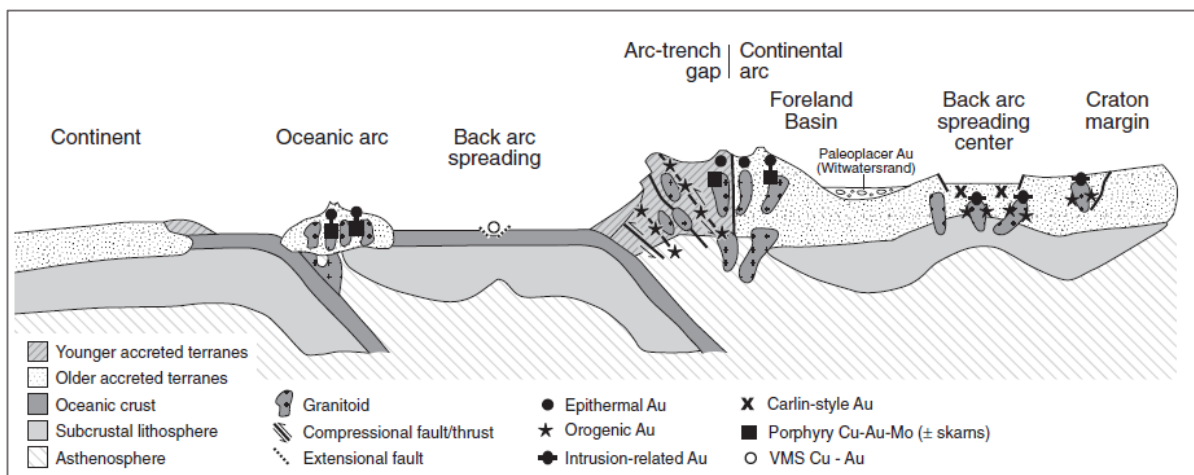


Fig. 5 : Schematic diagram showing the tectonic setting of various gold deposit types. Orogenic gold deposits develop in fore arc region of a convergent continental margin over a wide range of crustal depths and may also develop in deformed back-arc sedimentary sequences seaward of the craton margin. After Groves et al. (2005)

Phanerozoic orogenic gold deposits formed in the fore-arc adjacent to a subduction-related continental arc though some may occur in deformed back-arc basins (e.g. Sukhoi Log, Russia; Bendigo, Australia) (Saunders et al. 2013; Goldfarb et al. 2001; Goldfarb et al. 2005). The hydrothermal systems forming the orogenic gold deposits in the Precambrian are poorly understood

compared to Phanerozoic deposits due to the difference between the Earth thermal budget and tectonic processes. The complexity of the Precambrian deposits involve spatial overlap of orogenic gold with other type of deposits, the “Archean type” subduction system, giant orogenic gold system overprinted by younger, etc.

There is a strong structural control related to the localisation of orogenic gold provinces. The deposits are spatially associated with steeply-dipping transcrustal fault systems that are parallel to the strike of the orogeny or the metamorphic belt. The major structures (1st order) are several hundred kilometers in length and several hundred meters wide. In the field they are defined by a series of closely spaced distinct faults reflecting multiple deformation events. The transcrustal fault zones form the main conduits that focus fluid flow (Cox 2005) and gold lodes are located along 2nd- and 3rd-order secondary faults. These secondary faults are dominated by brittle-ductile to ductile shear zones, however gold bearing extensional veins may also develop but it is less common. The deposits forms generally in fault and shear zones at crustal levels within and above the brittle ductile transition zone, at depths of 3 to 12 km and temperatures ranging from 200° to 400°C. The variety of lithologies in greenstone belts and metasedimentary terranes result in differences in physical properties of the host rock (competent and non-competent rocks) serving as favourable host rocks, particularly in areas of minimum mean stress, such as fault jogs, fault bends, and fold hinges. The ore-bearing quartz-carbonate veins are commonly laminated or contain breccia fragments, which reflect repeated fracturing and fracture sealing in the hydrothermal systems over periods of a few million years (Cox 2005).

Several genetic models for the formation of orogenic gold deposits have been proposed due to the difficulties to identify a unique source of Au and ore-forming fluids. Moritz (2000) summarise them as follows: (1) granulitisation of the lower crust caused by CO₂-enriched fluids from the mantle followed by felsic magmatism (Fyon et al. 1989; Hodgson & Hamilton 1989); (2) magmatic fluids separation from tonalite - trondjemite - granodioritic intrusions (Burrows & Spooner 1987); (3) fluids produced by metamorphic devolatilisation (Kontak et al. 1990; Phillips & Powell 1993; Kerrich & Cassidy 1994); and (4) deep circulation of meteoric water (Nesbitt et al. 1986; Boiron et al. 1996). Furthermore, lamprophyres have also been suggested as a source for gold and ore-forming fluids, but Rock et al. (1989) has indicated that their association with orogenic gold deposits is limited to only structural relationship.

The majority of authors currently relate the genesis of orogenic gold deposit to metamorphic devolatilisation, however, there is still a debate about how these processes occur and focus gold bearing fluids to form a deposit. Nearly all orogenic gold deposits occur syn to post-peak metamorphism. Some of the large Precambrian deposits sit in high-grade metamorphic rocks (e.g., Hemlo in Canada, Challenger and Big Bell in Australia) formed during greenschist facies events on a prograde metamorphic path (Saunders et al. 2013; Phillips & Powell 2010). These could be the result of multiple or overlapping metamorphic events affecting the same region (Saunders et al. 2013). Amongst the others, the critical factors supporting the metamorphic model are: (1) the common fluid species H₂O–CO₂–CH₄–N₂–H₂S, low salinity fluid characteristic to products of metamorphic devolatilisation; (2) the heavy isotopes values of δ¹⁸O and δD for hydrothermal minerals (Goldfarb et

al. 1991; Kerrich 1989); (3) the varying $\delta^{34}\text{S}$ values reflecting variable host terranes going through a regional metamorphism (Goldfarb et al. 1997); and (4) the general depletion of Au and associated element in high-grade metamorphic rocks as they are at relatively high temperatures and most mobile S and Au would have already been removed from the rock sequence (Pitcairn et al. 2006).

3c. Ore forming system - source to sink

The widely accepted genetic model involving metamorphic devolatilisation (Fig. 6A&B) suggests that fluids are produced during greenschist to amphibolite facies metamorphic reactions in sedimentary

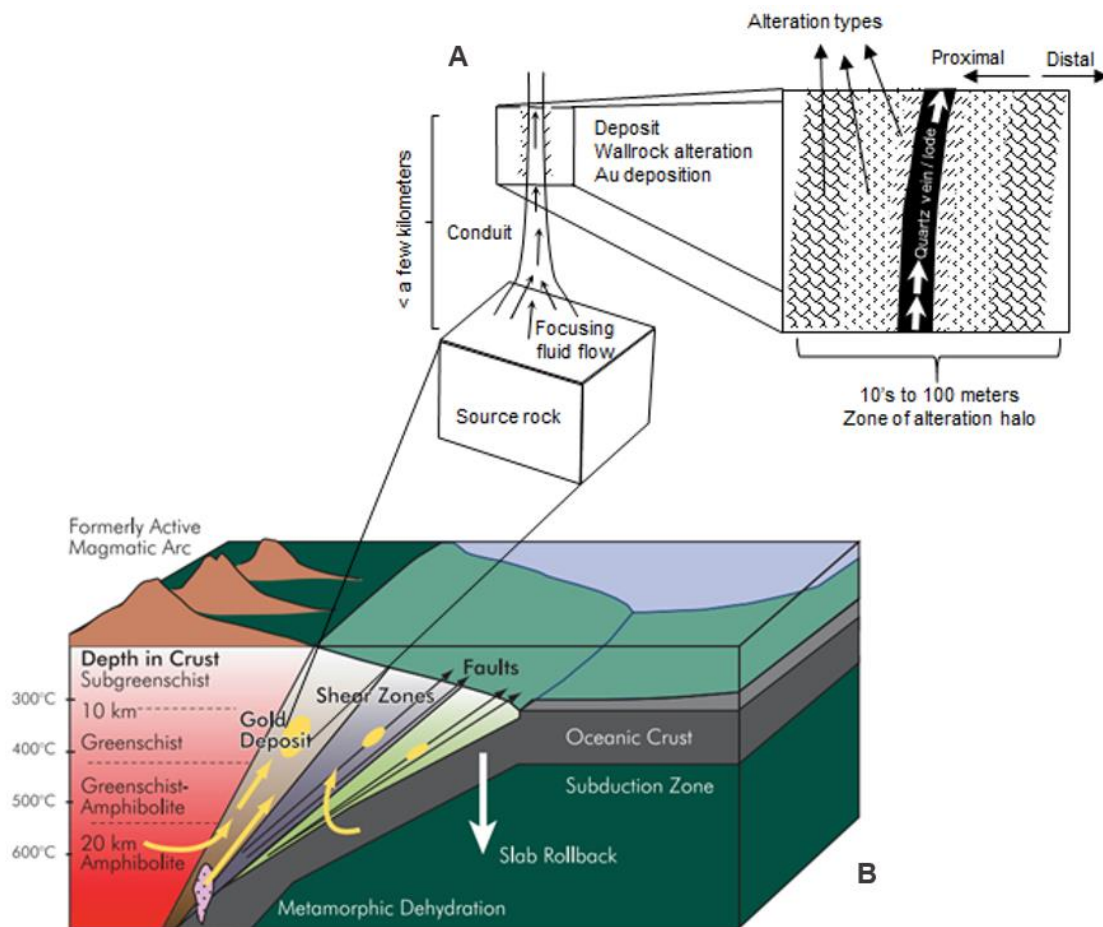


Fig. 6: A. Schematic architecture of lode gold hydrothermal system from the source to sink and formation of the ore deposit. Single-pass fluid flow is focused from a large volume of source rock (crustal block) from which gold is leached and may travel over several kilometres along channel ways to the deposits (trap which may be physical ore chemical). At the deposit, the fluid is constrained to a relatively narrow channel ways, with the formation of alteration halos as a result of fluid dispersion into adjacent wall rock (modified after Ridley & Diamond 2000). B. Cordilleran-type orogeny recognised for the widespread distribution of orogenic gold deposits in metamorphosed juvenile rocks on either side of the magmatic arc. The metalliferous fluids are focused along major crustal shear zones in the fore arc, which previously may have been sites of terrane suturing (after Kerrich 2005).

and volcanic rock sequences at temperatures of $\sim 440^{\circ}\text{C}$ – 520°C (Phillips & Powell 2010), with possibly 3–5 vol% of the rock (hydrated fraction and volatiles) converted into a hydrothermal fluid (Saunders et al. 2013). The hydrothermal fluid generates its own permeability due to fluids pressure (Tenthorey & Cox 2003) then migrate upward along transcrustal faults during episodic seismic events controlled by the fluids themselves and the activation or reactivation of the fault (Sibson et al. 1988).

Gold and associated metals are carried with the hydrothermal fluid to shallower level in the host rock already on a retrograde metamorphic path in greenschist facies at the brittle-ductile transition (Stüwe 1998). Gold is transported as a hydrosulfide complex AuHS^0 and $\text{Au}(\text{HS})_2^-$ in hydrothermal solutions systems at low temperature and pH ~5-6 and as $\text{Au}(\text{Cl})_2^-$ in system rich in Cl and low pH conditions at temperature above 400°C (Zhu et al. 2011).

In Phanerozoic orogenic gold deposits the source of gold is assumed to be the metasedimentary host rock itself (Pitcairn et al. 2006) and in Archean deposits, the source is thought to be dehydrating metabasaltic rocks, or widely distributed chert beds (Phillips & Powell 2010). Although some authors have debated for the need of a gold-enriched protolith to be metamorphosed to greenschist facies to form large gold provinces it appears that adequate fluid and sulfur budgets should ensure the viability of the ore system and a specific favorable gold-rich source horizon is not essential. However the ore system still need to be efficient to form economically exploitable deposits (Saunders et al. 2013). The migration of the fluids from the source area is followed by a precipitation or sink in a trap from where the deposit will start forming. The trap can be either physical or chemical. The physical traps may be formed by a host rock formed by a succession of competent and incompetent units and the chemical traps may be formed by Fe-rich host rocks that will cause sulphidation of the ore fluids and precipitate Au or Carbon rich rocks that may reduce the ore fluids and precipitate Au.

3d. Alteration - proximal and distal

Wallrock alteration in Phanerozoic gold deposits is common with alteration and geochemical haloes enveloping most of the deposits. Previous studies show that these alteration patterns can be significant targets in gold exploration at regional, district and local scale (Kishida & Kerrich 1987). The alteration haloes are caused by the interaction between the ore fluids and the wallrock which changes the chemistry and mineralogy of the wallrock in a systematic way (Fig. 6B). The extent and magnitude of the wallrock alteration halo depends on the state of deformation of the host rock, porosity and permeability of the host rock and the degree of chemical reactivity of the host (Bierlein et al. 1998). Therefore wallrock alteration although quite commonly visible, may be either extensive or weakly developed. Hydrothermal fluids in near-equilibrium with host-rock for most of the chemical components may also result in very weak developed wallrock alteration halo (Goldfarb & Miller 1997). The alteration assemblage varies in deposits hosted in greenschist facies and amphibolite facies host rock. The vast majority of orogenic gold deposits formed during the Phanerozoic are hosted in greenschist facies rocks (Goldfarb et al. 2001). The alteration sequence can reflect both the intensity of alteration (proximal to distal) and also the composition of wallrock. The different alteration types include: chloritisation, carbonation, (de-)silicification, sericitisation, albitisation and tourmalinisation. In greenschist facies deposits, the alteration assemblage is commonly characterised by the following alteration type distal to proximal: calcite-chlorite, calcite-dolomite and sericite (Eilu et al. 1998). Additionally sulfides alteration mostly involving pyrite and arsenopyrite is common, although due to extensive occurrence of pyrite in wallrock, it is difficult to establish the extent of hydrothermal pyrite

halo with accuracy (Bierlein et al. 1998). Other alteration minerals such as tourmaline and stibnite are present in some deposits (Gao et al. 1995).

The mineralogical and geochemical changes across the alteration sequence are generally gradual. A summary of the paragenetic alteration sequence commonly present around orogenic gold deposits hosted in metasedimentary rocks at greenschist facies condition is presented in (Fig. 7) and Table 1 shows the main features of alteration zones visible in hand specimen.

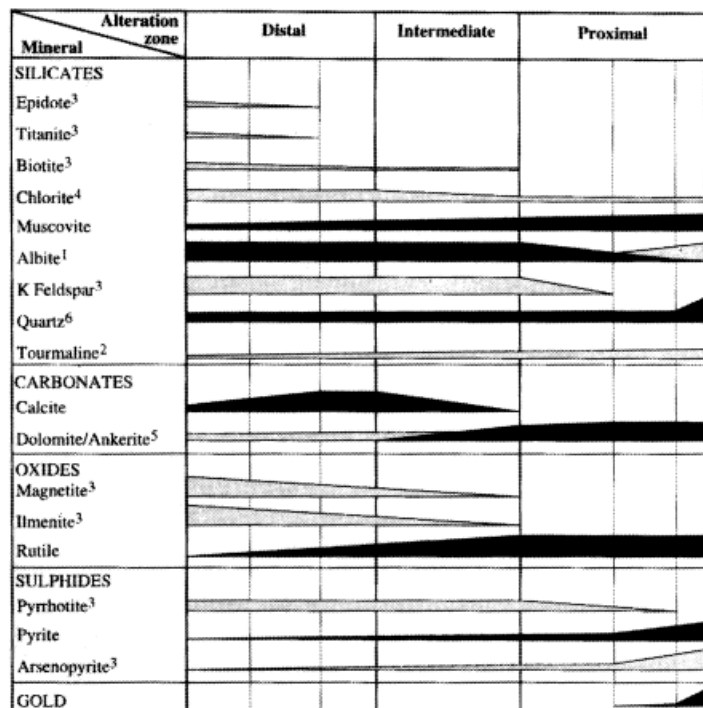


Fig. 7: Schematic summary of the paragenetic alteration sequence around orogenic gold deposits hosted in metasedimentary rocks at greenschist facies. Black ranges indicates where the minerals normally are present; grey ranges indicates less common cases. Proximity to mineralisation increase to the right. After (Eilu et al 1998).

1. There is locally significant albite formation in the area of most proximal alteration
2. The extend of tourmaline formation is unclear, as tourmaline is not present in all alteration envelopes
3. This mineral is present in highly variable amounts; the extent and the volume of arsenopyrite may be the same or even exceed that of pyrite.
4. Chlorite is present in highly variable amounts and may also be part of the proximal assemblage if muscovite is not present.
5. Dolomite instead of calcite, may occur in the distal alteration zones in some metasedimentary rocks areas.
6. Proximal silicification may be only easily detected indication of alteration around some deposits.

4. Sampling

A total of 131 drill core samples were collected at the Blackwater deposit in Reefton on the drill core W21 and W21c of which 72 samples were selected for geochemical and mineralogical analysis. The sample suite comprises metagraywacke and argillite of the Greenland Group and includes: protolith, distal, proximal and ore bearing (Au quartz lodes) samples. 25 samples selected in the upper section of the sampled core were used to estimate the protolith composition of the host rock and background concentration of various elements of interest. Two samples were systematically collected at each sampling point, one per lithological unit, in interval of ~50 meters. The 25 protolith samples are located more than 300 meters above the ore. The distal samples suite consists of the series of rocks between 300 meters and 12 meters away from the ore samples. High resolution sampling (every meter) was carried out for the proximal samples suite and cover the sequence of rocks located 10 meters above the ore and about 25 meters below the ore bearing samples.

Table 1: Main features of alteration zones identifiable in hand specimen in alteration sequences surrounding orogenic gold deposits hosted in metamorphosed and altered sediments at greenschist facies conditions. (Eilu et al. 1998)

Zone	Hand specimen features	Colour
Unaltered rock	Generally massive, primary sedimentary features are visible. Reaction with dilute HCl only in relatively scarce calcite-bearing veins and in calcite-bearing inter-pillow breccia.	Variable
Distal	Generally massive the primary sedimentary features are visible, Foliated texture is only present where the alteration zone occurs in a shear zone. Distinct reaction occurs with dilute HCl through the rock, except in cases of very fine grained rock which is characterised by more abundant carbonate ± quartz veins than coarser-grained types. Carbonate-quartz veins are characteristic in all rock types. Epidote may be present and visible in the most distal parts of the zone.	Generally similar to that of unaltered rock. Originally very dark rock may be slightly bleached if carbonation is intense.
intermediate	Primary sedimentary features are visible in areas of massive and weakly foliated texture. Distinct reaction with dilute HCl occurs throughout the rock. Fresh rock is not possible to distinguish from distal zone type without carbonate staining. The volume of carbonate-quartz veins and sulfides, and the degree of brecciation and foliation are higher than in the distal zone	Fresh rocks as in distal zone, but yellowish due to weak weathering of Fe-bearing carbonate if exposed to at the surface or to air.
Proximal	Intensely foliated and/or brecciated, massive only in domains of purely brittle deformation. The bleached colour combined with abundant sulfides (pyrite, pyrrhotite, and arsenopyrite) is the most distinctive feature. There is no reaction with dilute HCl or it reacts only in the rare post-gold mineralisation calcite-quartz veins. The volume of carbonate-quartz veins and sulfides is much greater than in other zones	Bleached appearance.

5. Analytical methods

XRF/LA-ICPMS

Whole rock analysis was carried out at Stockholm University by X-Ray Fluorescence (XRF) for major oxides and *Laser Ablation* Inductively Coupled Plasma Mass Spectrometry (LA-ICPMS) for trace elements. Both analyses were performed on fused-glass discs with a fuser-sample ratio of LiBo: 5g / sample: 2g. XRF analyses were performed using ZSX Rigaku Primus II X-Ray Fluorescence spectrometer and calibration was carried out using the standard material AGV-2. LA-ICPMS was performed by means of 193 nm ArF excimer laser coupled to a quadrupole Thermo X-Series II mass spectrometer. The analytical settings were: beam size 150µm, laser frequency and density respectively 10Hz and 7.5J/cm², Nitrogen flow rate 3.0ml/min. Accuracy and precision were assessed via external standard material NIST612a and BCR2 was analysed as known-unknown and result matched published values within ~10%. The internal standard used was ²⁹Si. 22 samples were

contaminated in W during samples preparation due to milling cup manufactured in tungsten carbide and W values for those samples are not reported.

Ultralow detection limit analysis for Au, As and Sb

Ultralow detection limit analysis were performed for Au via ICPMS using a Thermo Xseries 2 mass spectrometer and for As and Sb via Analytical Millenium Excalibur hydride generation atomic fluorescence spectrometer (HG-AFS) with a detection limit of 10ppt (part per trillion) following the method as described in Pitcairn et al. (2006). Analytical precision was controlled by analysing 4 duplicates samples and analytical accuracy was controlled by means of standard material TDB1, WMS and CH4. As and Sb values were compared with values obtained by LA-ICPMS on the glass discs, the binary plot As_{ICPMS} vs As_{AFS} yield a trend line with a slope of is 0.76 indicating that ICPMS data is 25% lower than the AFS data. This is most likely because As is lost during the glass discs making process. The binary plot Sb_{ICPMS} vs Sb_{AFS} data appears to have 2 trends - at low Sb content the trend is steeper and closer to 1:1 but at higher Sb content the trend has a much flatter slope showing that Sb is lost in the ICPMS analysis on glass discs. The trend line through all the Sb data has a slope of 0.26 indicating that the ICPMS data is 74% lower than AFS data.

***In-situ* LA-ICPMS**

In-situ trace elements analysis on sulfides minerals in thin sections were performed at the Department of Geology at University of Gothenburg. Analysis was performed using an Agilent 8800QQQ triple Quad ICPMS coupled with a New Wave NWR213 laser ablation system. The analytical conditions were: laser beam energy 5.5J/cm², spot size 30µm and 10µm respectively for large crystals and small crystal and Helium flow rate 900 ml/min. The isotopes measured were: Al²⁷, Si²⁹, S³⁴, Mn⁵⁵, Fe⁵⁷, Co⁵⁹, Ni⁶⁰, Cu⁶³, Zn⁶⁶, Ga⁶⁹, Ge⁷², As⁷⁵, Se⁷⁷, Mo⁹⁵, Ag¹⁰⁷, Cd¹¹¹, In¹¹⁵, Sn¹¹⁸, Sb¹²¹, Te¹²⁵, W¹⁸², Re¹⁸⁵, Au¹⁹⁷, Hg²⁰², Tl²⁰⁵, Pb²⁰⁸, Bi²⁰⁹ for analysis with the 30 µm spot size and Al²⁷, S³⁴, Fe⁵⁷, Co⁵⁹, Ni⁶⁰, Cu⁶³, Zn⁶⁶, As⁷⁵, Ag¹⁰⁷, Cd¹¹¹, Sb¹²¹, Au¹⁹⁷, Pb²⁰⁸ for analysis with the 10 µm spot size. Analytical accuracy was controlled with standard material Po275 and Onuk for sphalerite and galena; standard material 610, USGS Mass-1 old, USGS Mass-1 nano, Al3, GSD, BAM5 for all other sulfides. Measurement calibration was done using Zn⁶⁶ from Onuk for sphalerite, Pb²⁰⁸ from Po275 for galena and Fe⁵⁷ from Mass-1 nano for all other sulfides phases. Some of the measurements returned mixed analysis due to small spot size.

SEM and Microscopy

Thin sections of 40 selected samples from the protolith zone, the hydrothermally altered zones (distal and proximal) and the ore zone were manufactured by Vancouver petrography in Canada. The thin sections were studied by petrographic microscope and scanning electron microscope (SEM) at Stockholm University to determine the mineralogy and mineral paragenesis of the samples. A Quanta FEG650 environmental scanning electron microscope (ESEM) equipped with a CBS detector was used to identify sulfides phases and elements concentration in sulfides with the following settings: Working distance 10mm, High vacuum, 20kV, spot size 4µm.

6. Results

6a. Lithochemochemistry

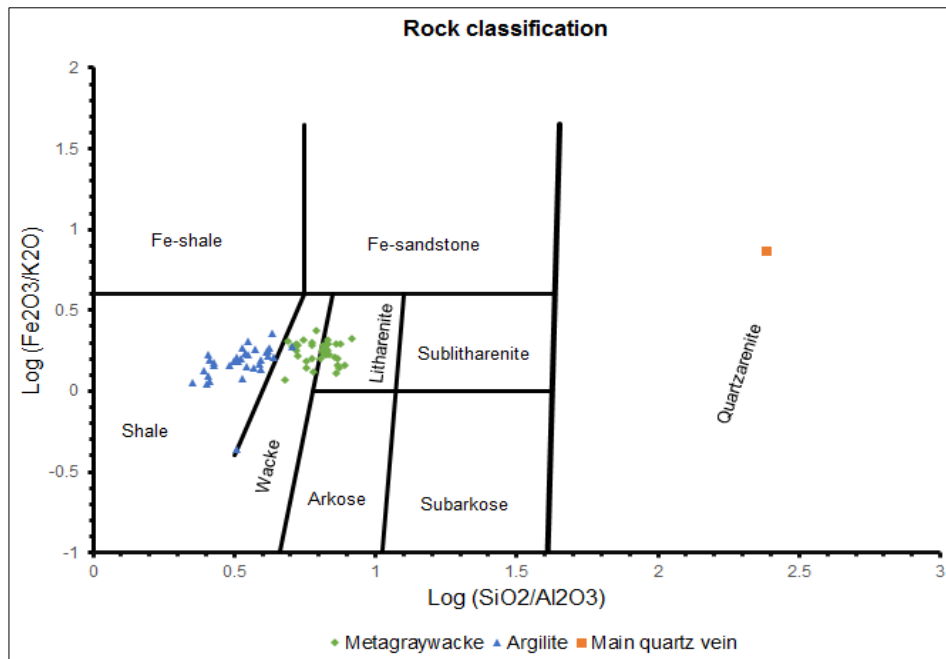


Fig. 8: Sediments classification. After Herron (1988)

The composition in major oxides in the samples collected suggests that the rocks are essentially shales, wackes and litharenites according to the Herron (1988) classification (Fig. 8). The data are reported in the electronic supplementary material 1 (ESM 1). These rocks have been metamorphosed to greenschist facies altering the shales to argillite and the wackes and litharenites to metagraywackes. The metagraywackes are fine to medium grain size metasediments and are unsorted or poorly sorted. The individual quartz grains are usually visible in the medium size grained unit as well as alteration minerals such as chlorite and sericite. The argillite is a slaty metamorphosed mudstone with very fine grain size exhibiting a well-developed cleavage. The argillite is much softer than the metagraywacke.

The argillite rocks show composition in major oxides within the following ranges: SiO_2 (53.34 – 68.00wt%), Al_2O_3 (15.52-23.71wt%), CaO (0.25-3.09wt%), MgO (2.34-4.56wt%), MnO (0.01-0.08wt%), P_2O_5 (0.05-0.11wt%), Fe_2O_3 (2.93-9.37wt%), Na_2O (0.00-1.80wt%), K_2O (3.08-8.08wt%), TiO_2 (0.71-0.93) and LOI@550 - loss on ignition at 550°C - (1.07-13.92wt%). The Metagraywacke shows in general lower Al_2O_3 , Fe_2O_3 , K_2O , LOI@550 and higher SiO_2 and CaO . The ranges of composition in major oxides for the metagraywacke are: SiO_2 (70.47-78.49wt%), Al_2O_3 (9.54-14.78wt%), CaO (0.45-5.50wt%), MgO (1.83-2.97wt%), MnO (0.02-0.26wt%), P_2O_5 (0.07-0.13wt%), Fe_2O_3 (3.68-5.93wt%), Na_2O (0.00-1.84wt%), K_2O (1.80-4.36wt%), TiO_2 (0.52-0.83wt%) and LOI@550 (1.13-10.77wt%). All XRF data are reported in ESM 2.

The concentration of Au, As and Sb in the argillite is in general higher than in the metagraywacke (Fig. 9). Given that Au, As and Sb are not homogeneously distributed in the rocks they sometimes show

high concentration even in the protolith samples resulting in the skewed distribution of these elements in the sample populations. Thus mostly the median and percentiles were used to compare the data instead of mean and standard deviation. The median concentrations of Au, As and Sb in the argillite are respectively 1.77 ppb, 21.57ppm and 3.39ppm; and in the metagraywacke 1.37 ppb, 13.97ppm and 2.88ppm.

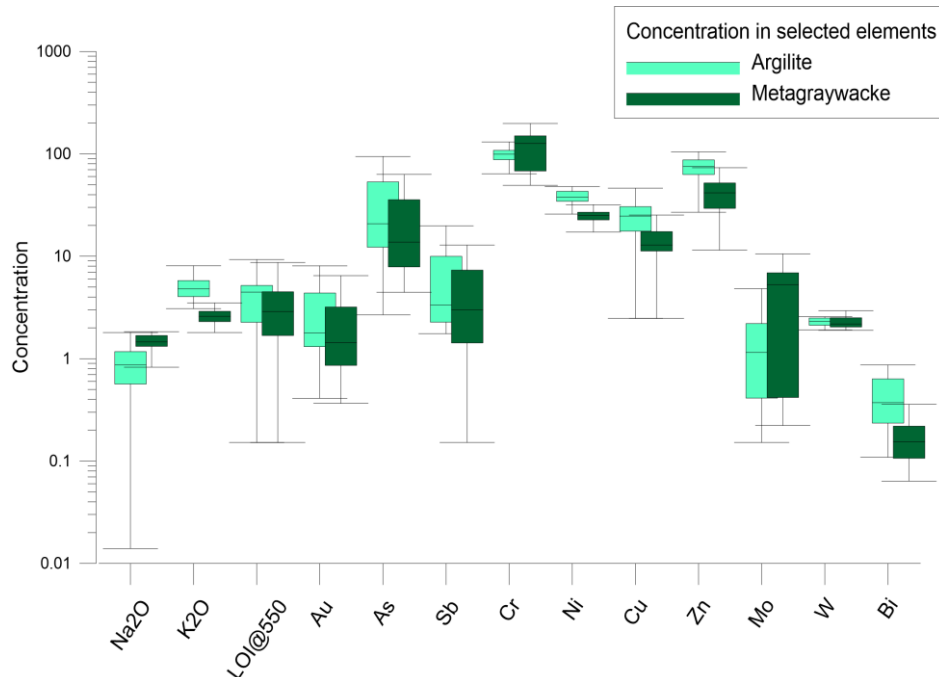


Fig. 9 : Box plot of abundance in Na₂O K₂O, LOI@550, Au, As, Sb, Cr, Ni, Cu, Zn, Mo, W and Bi in all the 72 samples collected on the drill core W21 and W21c at Blackwater. The middle line represent the median value, the upper and lower limit of the box represent respectively the 3rd quartile and 1st quartile and the upper and lower limit of the whiskers are the maximum and minimum values.

Other Au related elements and base metals concentrations (W, Bi, Mo, Ni, Cu, Cr and Pb) show 2 different styles of behaviour (ESM 3). Bi, Cr, Mo, Pb and W have their peak concentrations of respectively 1.71ppm, 472ppm, 31.56ppm, 116ppm and 5.1ppm in/or proximal to the main Au quartz vein. Whereas Cu, Ni and Zn show their lowest concentration of respectively 63.76ppm, 47.86ppm, 203ppm in/or proximal to the main Au quartz vein. There is a strong lithological control on major and trace elements concentration, with higher metal content in the argillite compared to the metagraywacke. Plots of concentration value downhole for selected elements are shown in the Fig. 10 and Fig. 11.

A statistical analysis was carried out to investigate the correlation between Au and related elements as well as other selected major oxides. The spearman rank correlation table (Table 3) shows that Au has commonly weak correlation with most of the elements analysed, a moderate positive correlation with Sb (spearman correlation coefficient $r_s=0.47$) and a moderate negative correlation with Na₂O ($r_s=0.42$). As exhibit a positive correlation with Sb ($r_s=0.77$), K₂O (r_s 0.48), Rb (r_s 0.46) and negative correlation with Na₂O ($r_s=-0.49$). Sb shows positive correlation with Rb ($r_s=0.52$) and K₂O ($r_s=0.55$) and a negative correlation with K₂O ($r_s=0.56$). The correlation coefficient matrix and the Spearman rank correlation table are reported in the ESM 4.

Na₂O and K₂O are the only major oxides showing moderate to strong correlation with Au and related elements as well as other selected base metals. Na₂O has commonly negative correlations and K₂O has typically positive correlations. The Spearman rank correlation coefficient as well as the p-value reflecting the significance of the correlation for a suite of selected elements is presented in **Error!**

Reference source not found..

Variable A	by Variable B	Spearman ρ	Prob> ρ
Ag	As	-0.0806	0.5007
Al ₂ O ₃	As	0.2321	0.0498
Ba	As	0.3571	0.0021
Bi	As	0.1237	0.3005
Cr	As	0.1517	0.2033
Cu	As	0.1759	0.1393
Fe ₂ O ₃	As	0.3302	0.0046
K ₂ O	As	0.4804	<.0001
LOI@550	As	0.2548	0.0307
MgO	As	0.2848	0.0153
Mo	As	0.0986	0.4101
Na ₂ O	As	-0.4944	<.0001
Rb	As	0.4607	<.0001
Sb	As	0.773	<.0001
SiO ₂	As	-0.3211	0.006
Sr	As	0.0449	0.7083
TiO ₂	As	0.2134	0.0719
W	As	0.4431	0.0013
Zn	As	0.3851	0.0008
Ag	Au	0.0166	0.89
Al ₂ O ₃	Au	0.1117	0.3502
As	Au	0.3492	0.0026
Ba	Au	0.1716	0.1495
Bi	Au	0.2627	0.0258
Cr	Au	0.0699	0.5596
Cu	Au	0.2015	0.0897
Fe ₂ O ₃	Au	0.1098	0.3588
K ₂ O	Au	0.2484	0.0354
LOI@550	Au	0.1124	0.3473
MgO	Au	0.0941	0.432
Mo	Au	0.052	0.6646
Na ₂ O	Au	-0.4223	0.0002
Ni	Au	0.1118	0.35
Pb	Au	0.2701	0.0217
Rb	Au	0.2287	0.0533

Sb	Au	0.4729	<.0001
SiO ₂	Au	-0.1541	0.1962
Sr	Au	0.0407	0.7343
TiO ₂	Au	0.1349	0.2586
W	Au	0.3283	0.0199
Zn	Au	0.1357	0.2556
Al ₂ O ₃	Bi	0.5617	<.0001
Ba	Bi	0.4994	<.0001
Cr	Bi	-0.2736	0.0201
Cu	Bi	0.5828	<.0001
Fe ₂ O ₃	Bi	0.5527	<.0001
K ₂ O	Bi	0.5027	<.0001
LOI@550	Bi	0.0839	0.4835
MgO	Bi	0.5759	<.0001
Na ₂ O	Bi	-0.2795	0.0174
Ni	Bi	0.5037	<.0001
Pb	Bi	0.5991	<.0001
Rb	Bi	0.4974	<.0001
SiO ₂	Bi	-0.5998	<.0001
Sr	Bi	-0.4099	0.0003
TiO ₂	Bi	0.4168	0.0003
Zn	Bi	0.5052	<.0001
Na ₂ O	Al ₂ O ₃	-0.463	<.0001
Na ₂ O	Fe ₂ O ₃	-0.4203	0.0002
Na ₂ O	MgO	-0.4537	<.0001
K ₂ O	Mo	-0.3544	0.0023
Na ₂ O	Mo	-0.0603	0.6149
K ₂ O	Na ₂ O	-0.6951	<.0001
Cu	Ni	0.5969	<.0001
K ₂ O	Rb	0.9895	<.0001
Na ₂ O	Rb	-0.6884	<.0001
Na ₂ O	W	-0.5332	<.0001
K ₂ O	Zn	0.7523	<.0001
Na ₂ O	Sb	-0.5556	<.0001
K ₂ O	Sb	0.5514	<.0001

Table 2: The Spearman rank correlation coefficient as well as the p-value showing the significance of the correlation for a suite of selected elements.

	Au	As	Sb	Mo	Ag	W	Bi	Cr	Ni	Cu	Zn	Rb	Sr	Ba	Pb	SiO2	Al2O3	MgO	Fe2O3	Na2O	K2O	TiO2	LOI@550	
Au	1.00																							
As	0.10	1.00																						
Sb	0.10	0.77	1.00																					
Mo	0.73	-0.06	-0.05	1.00																				
Ag	0.04	-0.19	-0.06	0.12	1.00																			
W	0.30	0.48	0.29	0.17	-0.28	1.00																		
Bi	0.33	0.12	0.28	0.08	0.14	-0.08	1.00																	
Cr	0.73	0.04	0.03	0.96	0.12	0.17	0.18	1.00																
Ni	-0.32	0.39	0.33	-0.55	-0.08	-0.03	0.30	-0.33	1.00															
Cu	-0.11	0.18	0.33	-0.36	-0.01	-0.10	0.44	-0.26	0.57	1.00														
Zn	-0.19	0.43	0.43	-0.35	0.06	0.05	0.24	-0.20	0.67	0.40	1.00													
Rb	-0.20	0.43	0.42	-0.48	-0.18	0.14	0.27	-0.31	0.75	0.42	0.56	1.00												
Sr	0.10	0.02	0.08	0.12	-0.03	0.23	-0.31	-0.05	-0.53	-0.20	-0.39	-0.23	1.00											
Ba	-0.18	0.31	0.34	-0.45	-0.16	0.09	0.21	-0.30	0.68	0.35	0.51	0.96	-0.20	1.00										
Pb	0.52	0.22	0.36	0.38	0.19	0.13	0.72	0.41	-0.07	0.16	0.09	0.00	-0.01	-0.04	1.00									
SiO2	0.38	-0.33	-0.32	0.68	0.11	0.01	-0.24	0.51	-0.88	-0.53	-0.61	-0.92	0.31	-0.88	0.12	1.00								
Al2O3	-0.37	0.27	0.29	-0.65	-0.12	-0.04	0.26	-0.47	0.87	0.49	0.61	0.93	-0.41	0.91	-0.12	-0.98	1.00							
MgO	-0.37	0.31	0.29	-0.66	-0.09	-0.05	0.28	-0.47	0.92	0.58	0.62	0.83	-0.39	0.79	-0.08	-0.97	0.94	1.00						
Fe2O3	-0.32	0.35	0.29	-0.61	-0.09	-0.07	0.32	-0.41	0.95	0.58	0.64	0.79	-0.51	0.73	-0.07	-0.94	0.92	0.98	1.00					
Na2O	-0.39	-0.57	-0.49	-0.15	0.18	-0.52	-0.30	-0.31	-0.39	-0.17	-0.33	-0.66	0.11	-0.62	-0.29	0.43	-0.44	-0.38	-0.37	1.00				
K2O	-0.19	0.52	0.50	-0.48	-0.17	0.14	0.26	-0.30	0.78	0.44	0.61	0.98	-0.24	0.94	0.02	-0.92	0.92	0.85	0.82	-0.68	1.00			
TiO2	-0.55	0.26	0.29	-0.78	-0.14	0.02	-0.04	-0.67	0.71	0.41	0.53	0.73	-0.21	0.71	-0.33	-0.83	0.83	0.75	0.73	-0.18	0.74	1.00		
LOI@550	-0.13	0.48	0.25	-0.25	-0.13	0.44	-0.02	-0.18	0.32	0.12	0.37	0.34	-0.19	0.22	-0.03	-0.32	0.30	0.30	0.35	-0.26	0.37	0.26	1.00	

Table 3 : Spearman rank correlation for selected elements analysed

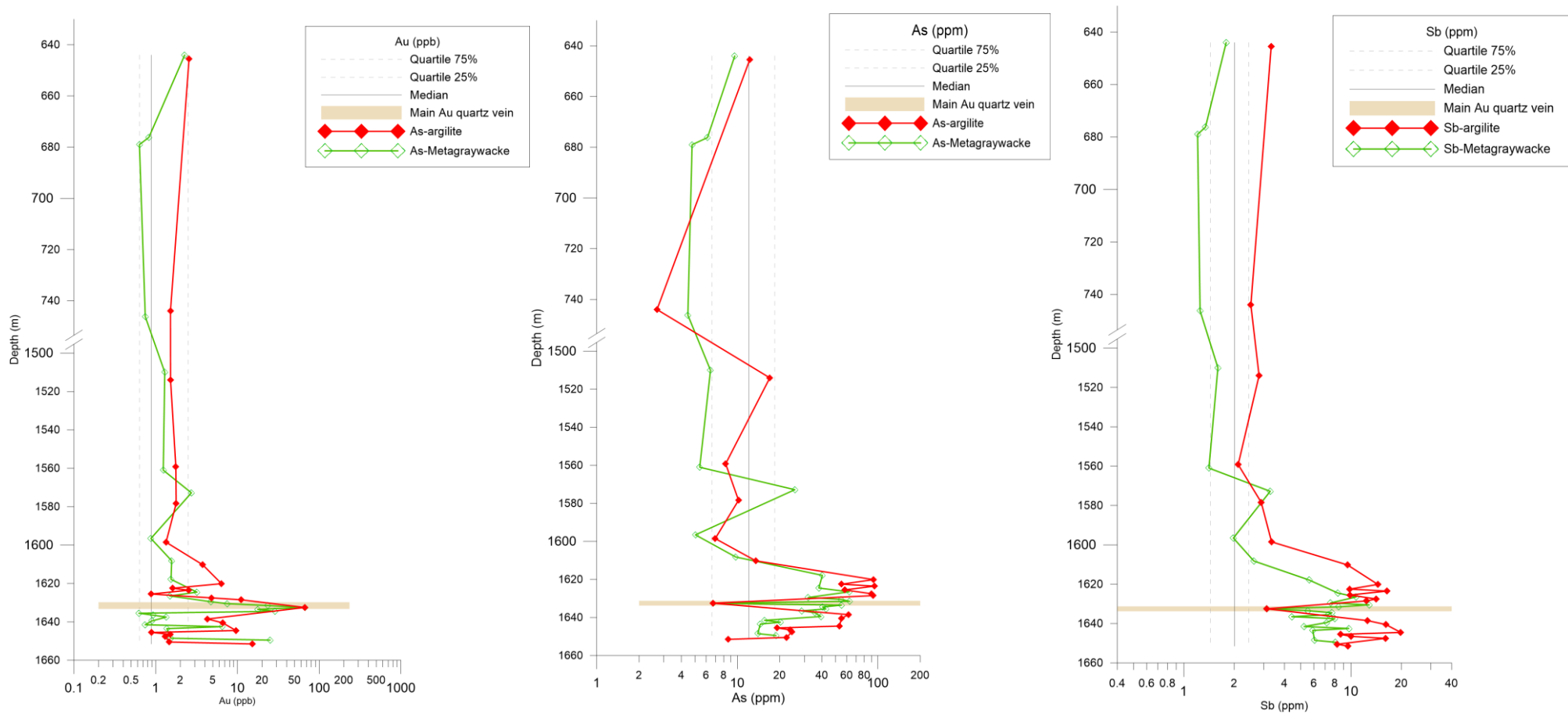


Fig. 10 : Concentration of Au, As and Sb downhole. The dashed grey line on the left and right represent the 1st quartile (25%) and 3rd quartile (75%), the middle line is the median.

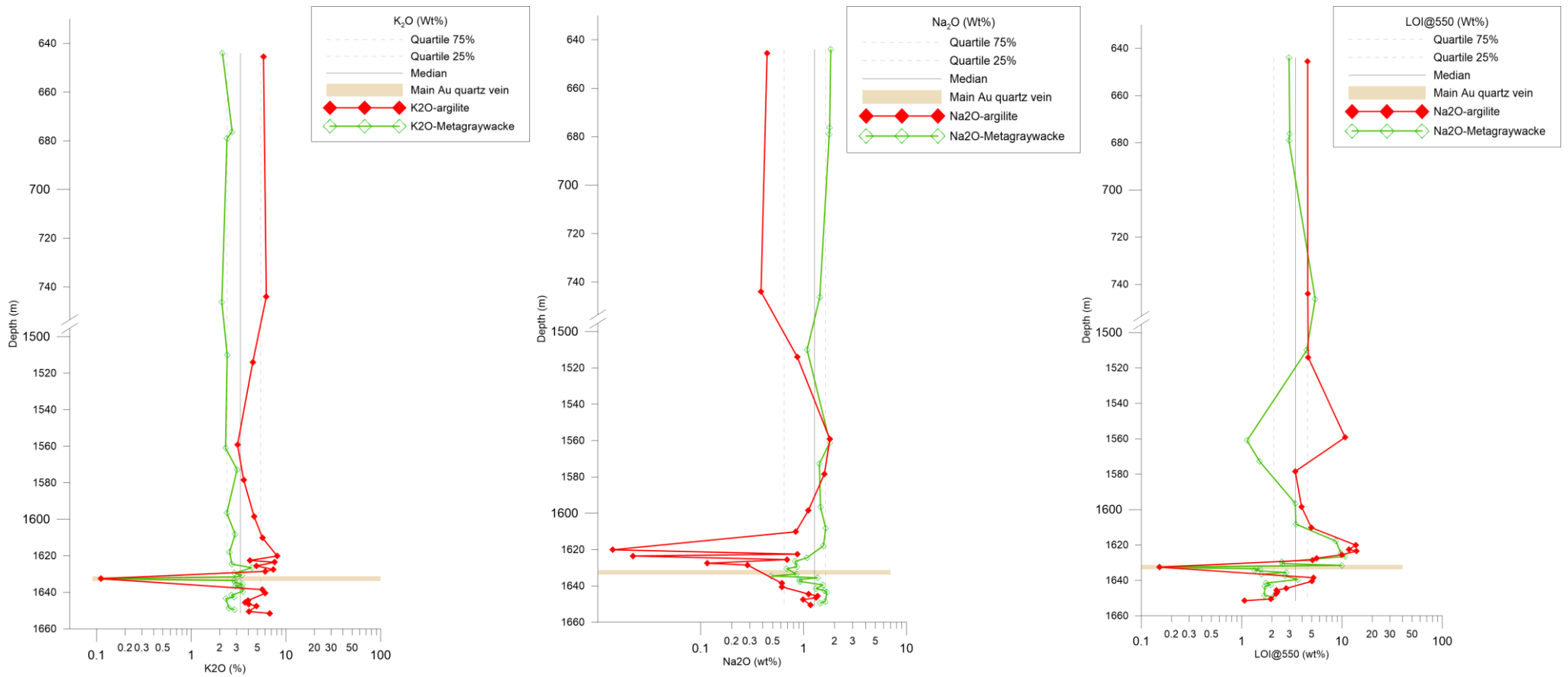


Fig. 11: Concentration of Na₂O, K₂O & LOI@550 downhole. The dashed grey line on the left and right represent the 1st quartile and 3rd quartile, the middle line is the median.

6b. Mineralogy

Wall rock alteration

The alteration sequence in the wall rock was divided in 4 alteration zones: The protolith (least altered zone), the distal alteration, the proximal alteration and ore zone alteration. These 4 alteration zones show noticeable mineralogical changes distal to proximal, indicating that the rock has undergone varying degrees of hydrothermal alteration. In the following description, the term “opaque mineral” is used to describe sulfides and all other opaque minerals in transmitted light, and “alteration mineral” is used to describe silicates and carbonates minerals that are visible in transmitted light.

Protolith

Alteration mineralogy

The typical mineral assemblage is quartz – chlorite – plagioclases (albite) – carbonates (mainly dolomite with minor calcite according to binary plot of molar ratio Ca/Ti versus CO₂/Ti – Fig. 14) – epidote (minor) – biotite (minor). The sedimentary textures are fairly well preserved (Fig. 13A). The argillite unit has commonly a very fine grained quartz bearing matrix. Chlorite present in the least altered samples is assumed to be part of the pre-alteration assemblage from the greenschist facies metamorphism that regionally affected Reefton prior hydrothermal alteration and mineralisation, although there may be a small amount of hydrothermal chlorite in the late cracks and veins. Because hydrothermal chlorite and metamorphic chlorite coexist it is difficult to estimate the extent of chloritisation caused by hydrothermal alteration. Quartz generally forms the fine-grained matrix but is also observed as anhedral recrystallised patches (Fig. 12A). The samples nearer to the distal alteration suite contain more chlorite and quartz filling pressure shadows around pyrite porphyroblasts

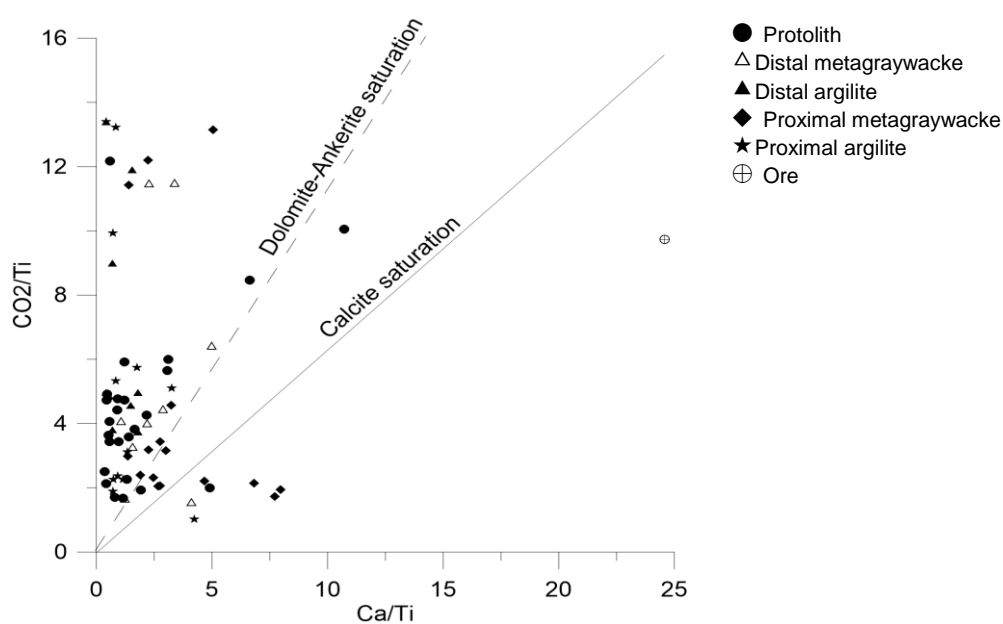


Fig. 12: Molar Ca/Ti versus CO₂/Ti. Most of the Blackwater samples are above the dolomite and ankerite saturation line, and a few samples plot below the calcite saturation line. Field boundaries are for molar CO₂/Ca ratios, which range from calcite (CO₂/Ca=1.0), ankerite–dolomite (CO₂/Ca=2.0) and magnesite–siderite (CO₂/Ca= infinity; Eilu et al. 1998)

or aggregates. Carbonates in the protolith samples are restricted to mostly quartz-carbonates composite veinlets and occur as disseminated grains in a few samples. Textural relationships between quartz filling pressure shadows and quartz carbonates (veins and rims merging in some cases) suggests that they may have formed at the same time. Other accessory phases present include phosphates (monazite, apatite and xenotime) and oxides (chromite, zircon and rutile) in variable amounts. Monazite and zircon are present as inclusions in the matrix while chromite forms patches and fringe some opaque minerals.

Opaque minerals

The main sulfides phases in the protolith samples are pyrite and chalcopyrite. Pyrite is scattered pervasively in the rock but it also occurs as isolated euhedral to subeuhedral grains or aggregates of euhedral porphyroblasts. Some of the pyrite porphyroblasts in the lower section of the protolith samples suite appear to have been boudinaged and rotated. The samples in the lower section of the protolith near the distal alteration suites have large crystals of zoned pyrite. The zoned pyrite has a solid core and a porous rim and in some cases an outer solid rim that is brighter. The zoning may be interpreted as both a repeated growth and low temperature formation from an impure fluids or metamorphic growth. Chalcopyrite is either coeval to pyrite, or in some samples partially replaces early pyrite. Others minor sulfides phases present include Galena that mostly occurs as inclusions in pyrite, and occasionally as coating in between aggregates of pyrite porphyroblasts or associated with chalcopyrite and sphalerite. Late cracks with lensoid shapes parallel to the foliation contains scattered and very small cobaltite grains. Rare sphalerite grains are generally sitting next to chalcopyrite. Tetradyomite (Bi_2TeS), is present in one sample only and is sitting next to chalcopyrite, and could be the result of mineral replacement. Minor amount of gersdorffite (NiAsS), millerite (NiS) and pentlandite ($(\text{Fe,Ni})_9\text{S}_8$) are present in one sample in the lower section of the protolith near the distal alteration zone.

Distal alteration zone

Alteration mineralogy

The primary sedimentary textures are sporadically preserved and small patches of bleached appearance of hydrothermal alteration begins to appear in the lower section of the distal sample suite near the proximal alteration zone. Well-developed foliation and crenulation cleavage are common (Fig. 13B). Chlorite and dolomite are the most common alteration minerals in the distal suite. The chlorite alteration is pervasive and extensive yielding typically a specific green colour. The mineral assemblage is quartz – carbonates (dolomite and siderite) – chlorite – plagioclases (albite) – biotite – muscovite (minor, mostly sericite in the lower section of the distal sample suite) - epidote – actinolite – tremolite in varying amount. The matrix is formed by finely to medium size quartz grains and patches of coarse recrystallised quartz are present. Pressure shadows of recrystallised quartz commonly fringes large euhedral to subeuhedral pyrite porphyroblasts. Composite quartz-carbonates veins is common and cross cut earlier quartz-only veins. Carbonate alteration is extensive in the matrix with appearance of carbonate-spotting in the lower section of the distal alteration zone. Sporadic

replacement reaction textures of chlorite being replaced by sericite can be observed. Oxides (Zircon, chromite and rutile) and phosphates (apatite, monazite and xenotime) phases are present in variable amount. Monazite forms mainly inclusions in the silicates matrix.

Opaque minerals

The main opaque minerals are pyrite and chalcopyrite commonly associated with various amount of galena, cobaltite, sphalerite, gersdorffite (NiAsS) and ullmannite (NiSbS). Pyrite grains are commonly zoned with often more than 1 overgrowth rim. This indicates repeated growth under different metamorphic or hydrothermal conditions. Patches of pyrite porphyroblasts are associated with chalcopyrite, cobaltite and sphalerite. Galena is present mostly as inclusion in pyrite and chalcopyrite or coating cracks in fractured pyrite. Sphalerite replaces chalcopyrite and shows replacement texture along grain boundaries. Euhedral to subeuhedral (Rhombohedral-Lozenge) shaped cobaltite grains are commonly associated with pyrite (intergrowth), galena, gersdorffite and ullmannite (Fig. 12C). Gersdorffite and ullmannite are only present in minor amount and may be coeval to cobaltite.

Proximal alteration zone

Alteration mineralogy

The main alteration style in the proximal zone is sericite and carbonate alteration. The bleaching appearance intensifies closer to the main quartz vein. Orange-brown carbonates spots are common (Fig. 13E). The mineral assemblage consists of quartz – muscovite (mostly sericite) - carbonates (siderite-ankerite) – chlorite - epidote - tremolite – actinolite - biotite (rare). Aggregates of opaque porphyroblasts are fringed by pressure shadow filled with quartz. Several composite quartz-carbonates veins cross-cutting the foliation are present implying the carbonates are late relative to the foliation (Fig. 13C). Sericite alteration is extensive occurring as both pervasive and fracture controlled. Replacement of plagioclases (albite) by sericite is common (Fig. 13G). Carbonates spots are frequent and occasionally have lensoid shapes parallel to the foliation or crenulation. Actinolite and tremolite are more common than in the distal alteration zone. Rutile, apatite and monazite are generally present in the matrix.

Opaque minerals

The main sulfides phases in the proximal alteration zone are pyrite, chalcopyrite, cobaltite, galena, sphalerite and gersdorffite. Ullmannite, pentlandite and millerite are present but in lesser quantities. Large crystals of pyrite are commonly zoned with three to four growth rims. Zoned pyrite has commonly a solid core, a first porous rim followed by alternating solid and porous rims. Aggregates of small euhedral pyrite crystals occur near large zoned pyrite. Pyrite (including zoned pyrite) exhibits vein and fracture replacement texture (Fig. 12B). Chalcopyrite and sphalerite are frequently replaced by silicates minerals. Chalcopyrite is texturally related to pyrite but is also usually associated with gersdorffite, sphalerite and cobaltite.

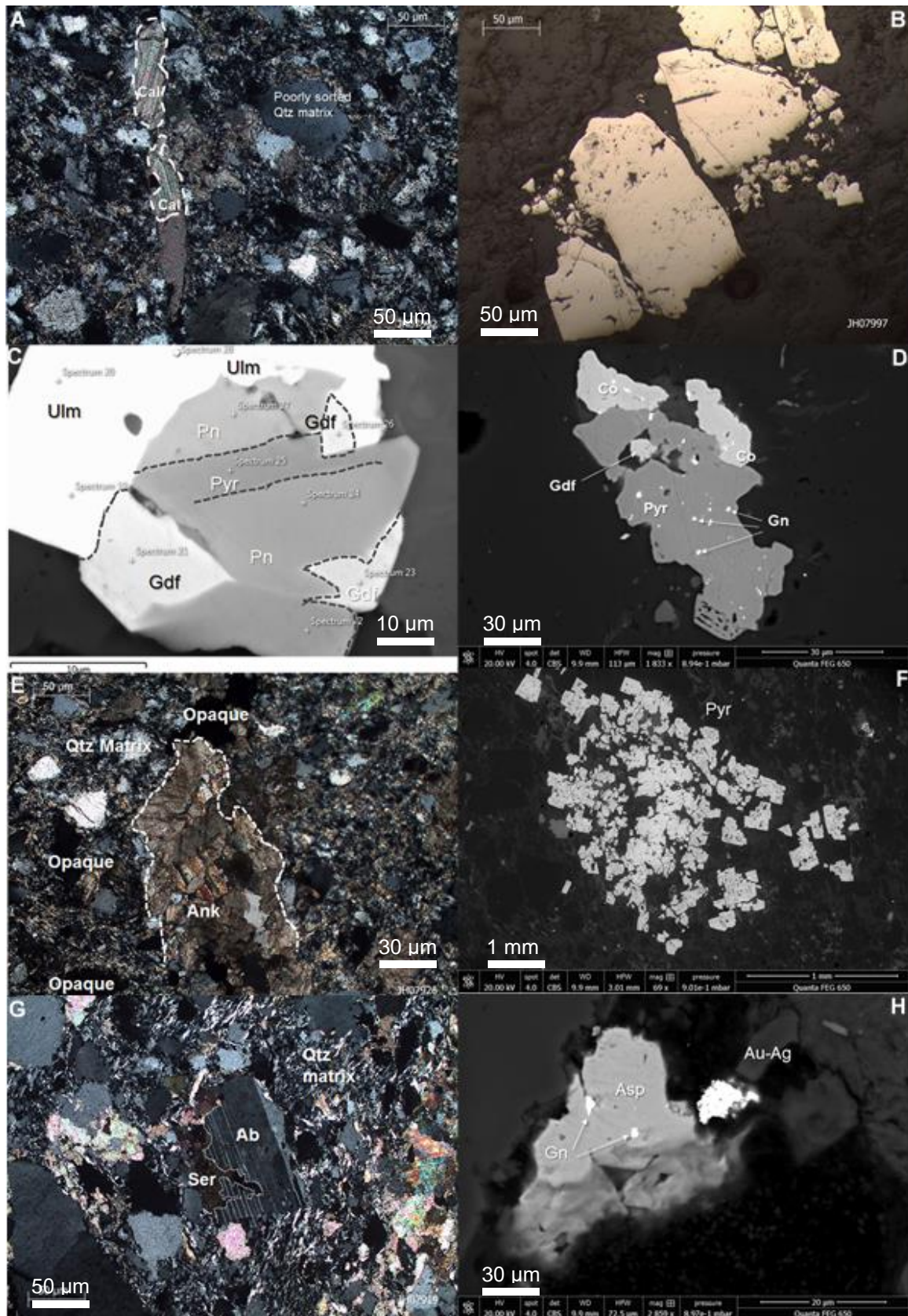


Fig. 13: Microscope images in transmitted light (A, E and G), reflected light (B) and SEM Photomicrographs (C, D, F and H). A. Calcite patches in quartz matrix (protolith); B. Pyrite porphyroblasts in protolith; C. Gersdorffite intergrowth in Pyrite associated with Ullmanite replacing pentlandite in distal sample; D. Galena and Gersdorffite inclusion in Pyrite associated cobaltite intergrowth in Pyrite; E. Ankeritic alteration in proximal alteration zone; F. Pyrite aggregate (advanced alteration) in proximal alteration zone; G. Reaction texture commonly observed in the proximal and ore zone of Plagioclase (Albite) being replaced by Sericite; H. Electrum (Au-Ag alloy) sitting next to arsenopyrite in the main Au quartz vein.

Galena is mostly filling pyrite cracks or sit next to the pyrite outer rim. Galena also form inclusions in pyrite and cobaltite and textural relationship indicate that it is a late phase compare to the pyrite, chalcopyrite and cobaltite. Cobaltite is mostly present in lensoid cracks in the matrix but also associated with aggregates of chalcopyrite. Intergrowth replacement texture of gersdorffite replacing chalcopyrite is common. In some cases gersdorffite partially surround chalcopyrite crystals suggesting a replacement guided by grains boundaries.

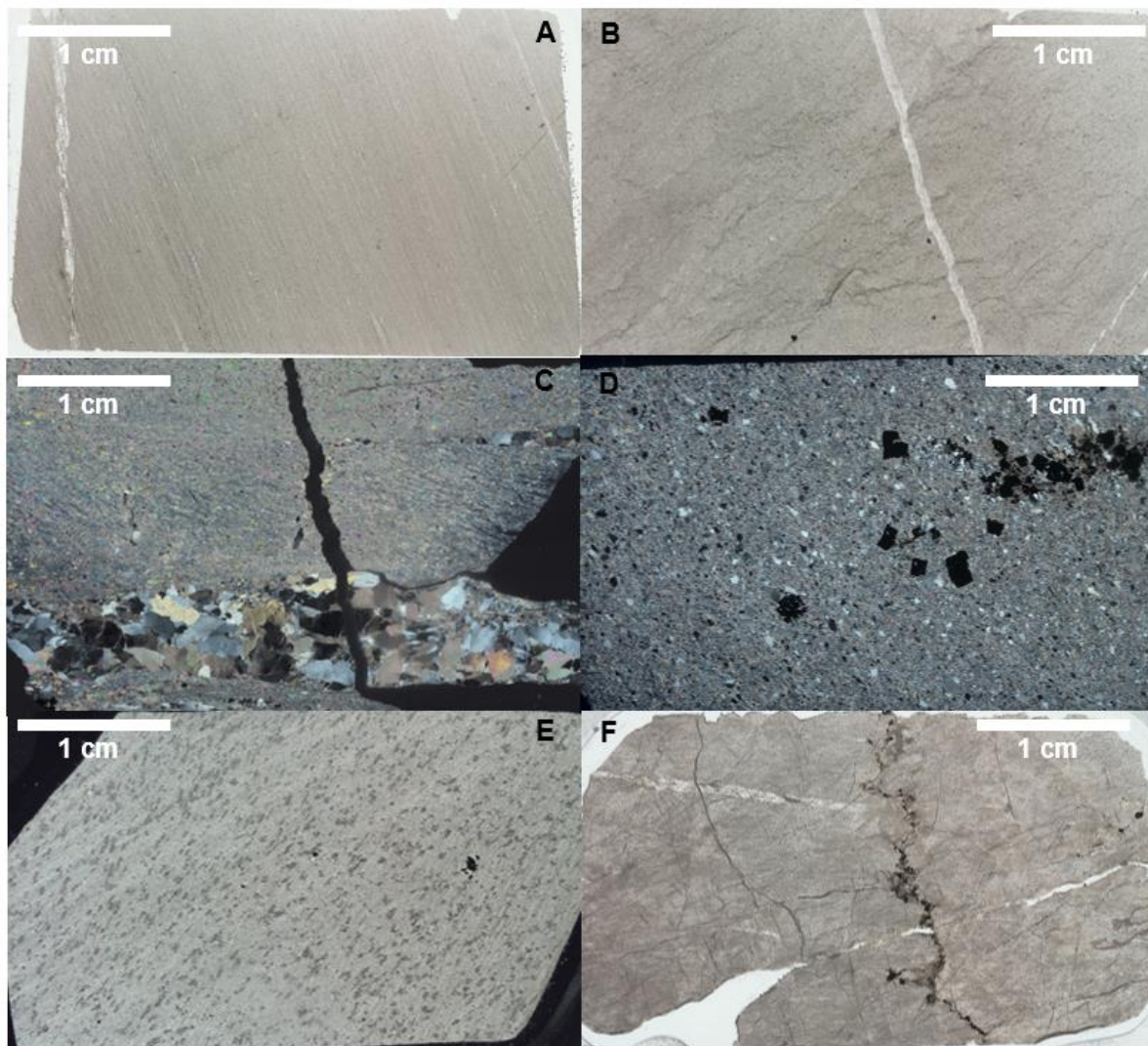


Fig. 14: Scans of polish thin sections. A) Sedimentary texture in protolith sample of the argillite unit – Sample JH07830; B. Crenulation cleavage along diagonal (upper right-lower left) in distal argillite sample JH07983; C. Composite quartz carbonates vein cross cut by a late quartz vein (extinct on the figure) – sample JH07901; D. Pyrite porphyroblasts (dark, opaque) rotated and boudinaged in proximal sample JH07919.; E. Carbonates spots in proximal sample JH07913; F. Main Au quartz vein with stylolitic veins (dark) cross cutting main quartz vein - electrum grains sitting next to arsenopyrite are present in the dark stylolitic vein. – sample JH07920.

Ore zone alteration

Alteration mineralogy

The main Au-bearing quartz vein is made of 80% to 90% of quartz. The main vein is white and banded and is cross cut by late grey quartz with stylolitic texture (Fig. 13F). In transmitted light the quartz appears as anhedral patches of very coarse grains associated with carbonates (ankerite),

muscovite (mostly sericite) and biotite spatially restricted to cracks and veins. Composite veinlets quartz-carbonates crosscut both the early white quartz and the late grey quartz stylolites. In the second ore sample quartz filling pressure shadow fringes large porphyroblasts of opaque minerals. Disseminated muscovite laths in the quartz matrix have been rotated and form inclusion in opaque minerals. Sericite is abundant compared to the rest of the core. Relicts of albite crystals being replaced by sericite are common. Carbonates and quartz filling pressure shadows surround euhedral porphyroblasts of opaque minerals. Minor and scattered epidote grains are present in the matrix. Phosphates (apatite and xenotime) and oxides (rutile) phases are present in varying amount.

Opaque minerals

A feature that is unique to the ore zone is the presence of arsenopyrite rather than cobaltite as the main As-bearing mineral. Arsenopyrite replaces pyrite and chalcopyrite and forms in between fragments of fractured pyrite. Au is present as electrum and is proximal to arsenopyrite in the main ore sample (Fig. 12H). Other main sulfides are pyrite, chalcopyrite, cobaltite, gersdorffite and galena. Sphalerite, pentlandite and millerite are present in minor extents. Pyrite porphyroblasts appear to have been rotated (Fig. 13D). Pyrite is mostly zoned pyrite with 2 to 3 generations of rims. Chalcopyrite commonly replaces pyrite. Sphalerite is generally associated with chalcopyrite. Galena forms inclusions in pyrite, chalcopyrite, arsenopyrite and cobaltite and in the matrix but it also forms joints filling between pieces of fractured pyrite grains. Pentlandite, millerite and gersdorffite form very small inclusions in Fe-Mg silicates. Millerite occurs as mineral replacement of pentlandite.

Mineral paragenesis synthesis

The paragenetic sequence presented here focuses on the relative timing of formation of minerals observed in the thin sections. Although structural consideration has been mentioned in the mineral description, the main focus of the mineralogical study was the mineral formation based on textural relationship between minerals. The paragenetic sequence is presented in Fig. 15.

6c. *In-situ* mineral chemistry

Distribution of Au, As and Sb in sulfides

Au – The concentration of Au in pyrite varies from 0.01ppm to 9.03ppm with a mean value of $(0.79 \pm 0.25 \text{ ppm}, n=59, 7 \text{ measurements were below limit of detection - bld})$. The highest Au abundance is found in Arsenopyrite which has Au concentrations ranging from 1.16ppm to 55.85ppm and a mean value of $12.59 \pm 7.33 \text{ ppm} (n=7)$. Measurements in cobaltite yield Au concentrations varying from 0.39ppm to 4.20ppm and an average concentration of $1.83 \pm 0.45 \text{ ppm} (n=8)$ and in galena Au abundance ranging from 0.14ppm to 4.71ppm with a mean value of $1.77 \pm 0.61 \text{ ppm}$. Chalcopyrite has Au concentrations mostly below detection limit with a maximum value of 0.4ppm. The lack of number of measurements in other sulfides phases present is mainly due to grain size being smaller than 10 μm . Alongside electrum which is present in the main ore vein, the main Au carriers are arsenopyrite and pyrite. A single measurement in pentlandite yielded a concentration of 9.91ppm (Fig. 16).

As – Arsenopyrite, cobaltite and gersdorffite are the main as bearing minerals. Measurements in arsenopyrite and cobaltite yield respective concentration ranges and mean values of: 40.76%-46.45% and 43.85±8.98% (n=7); 42.94%-51.56% and 47.39±10.42% (n=7). Only 1 measurement yielding a concentration of 51.60% in gersdorffite was reported the other 4 measurements returned mixed result due to small grain size. The average concentration of As in pyrite, chalcopyrite and galena is 2045±260 (n=64); 137.42±51.81ppm (n=12) and 694±285ppm respectively. In addition to the main As-bearing minerals (arsenopyrite, cobaltite, gersdorffite) at Blackwater (Fig. 16), pyrite is also

Minerals	Zone	Least altered (Protolith) Pre-alteration assemblage	Distal	Proximal	Main Au quartz vein
Silicates					
Assemblages typical for each alteration zones					
Quartz		██████████	██████████	██████████	██████████
Quartz only vein			-----	-----	██████████
Quartz-carbonates veins			-----	-----	██████████
Chlorite		-----	-----	-----
Muscovite			-----	-----	-----
Sericite			██████████	██████████
Albite – (plagioclases)		-----		
Epidote			-----
Tremolite			-----
Actinolite			-----
Biotite			-----
Carbonates					
Calcite		-----			
Dolomite		-----	-----		
Ankerite				-----	
Siderite			-----	-----	
Sulfides					
Pyrite		██████████	██████████	██████████	██████████
Rim 1			-----	-----	██████████
Rim 2			-----	-----	██████████
Rim 3			-----	-----	██████████
Gold (Electrum)				
Arsenopyrite					-----
Chalcopyrite		-----	-----	-----	-----
Cobaltite			-----	-----	-----
Galena			-----	-----	-----
Gersdorffite			-----	-----	-----
Ullmanite			-----	-----	
Millerite					-----
Pentlandite				-----	-----
Sphalerite			-----	-----	-----
Tetradymite				
Oxides					
Zircon		-----	-----	-----
Chromite		-----	-----		
Rutile		-----	-----	-----	-----
Phosphates					
Apatite		-----	-----	-----	-----
Monazite		-----	-----	-----	-----
Xenotime		-----	-----	-----	-----

██████████ Major or ubiquitous
 ----- Common
 ----- Uncommon
 ----- Local or in minor amount
 Rare

Fig. 15: Mineral paragenesis of Blackwater

enriched in As (concentration ranging from 43.26ppm to 10031ppm, n=61 with 3 measurements bld). Chalcopyrite exhibits a relatively lower enrichment than pyrite (2.56ppm to 642ppm, n=12 with 3 measurements bld).

Sb – The highest concentrations of Sb are found in gersdorffite (2528ppm) and cobaltite (21514ppm) this is most likely due to lattice substitution of As by Sb. Arsenopyrite, cobaltite, pyrite, chalcopyrite, galena and sphalerite have respectively a mean concentration of: 263 ± 43.76 ppm (n=9), 3285 ± 2608 ppm (n=8), 60.17 ± 13.36 ppm (n=61), 16.07 ± 3.76 ppm (n=16), 22.13 ± 9.78 ppm (n=8) and 42.91 ± 30.57 ppm (n=3). Beside gersdorffite and cobaltite, other common sulfides at Blackwater have fairly low Sb concentration and this is also observed in whole rock analysis profile. The main Sb-bearing mineral observed in thin section is Ullmanite however it is not a common mineral phase and no analysis was possible due to the small size of grains. Noticeable Sb enrichment is observed in Arsenopyrite, pyrite and in a lesser extent in chalcopyrite (Fig16).

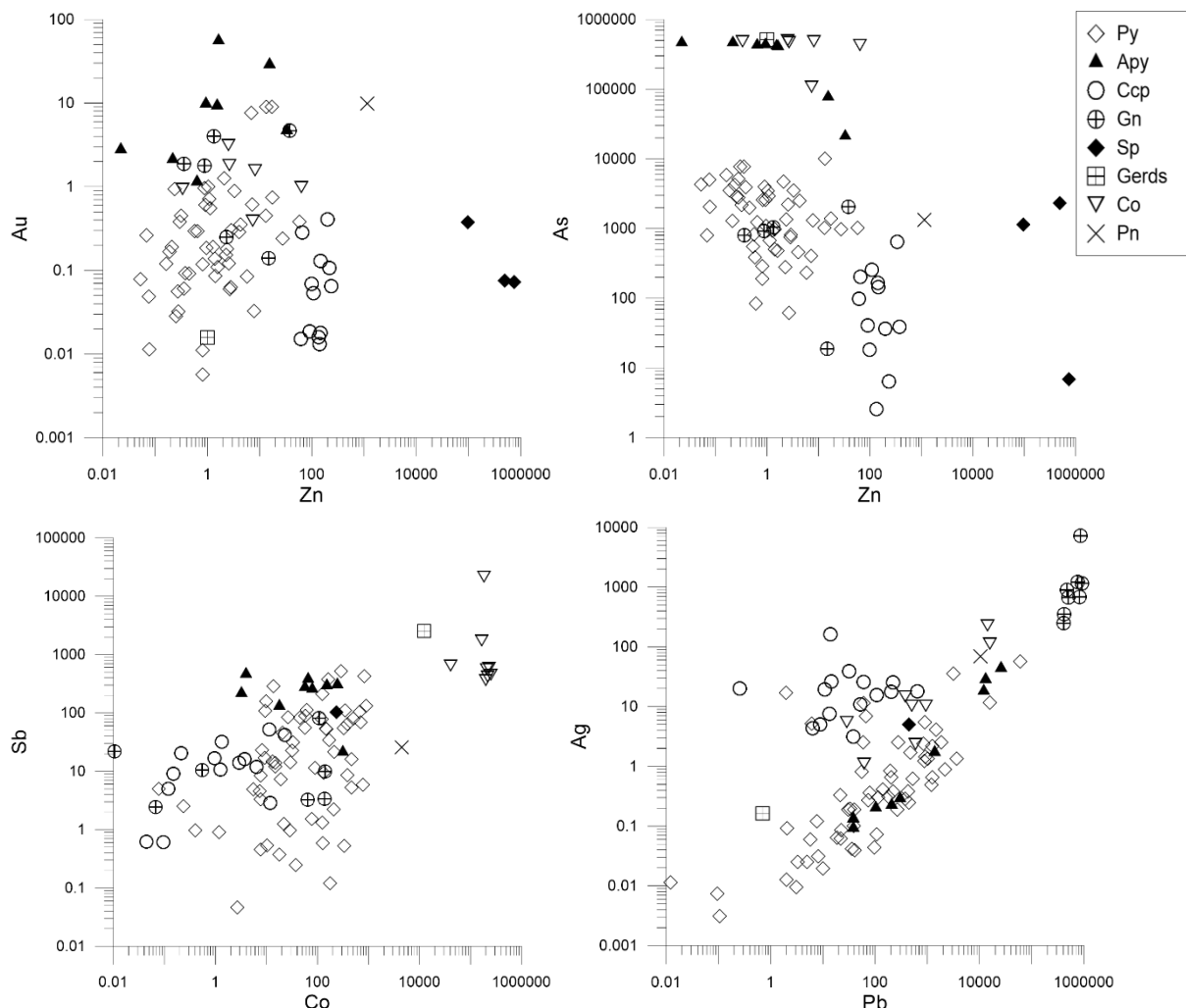


Fig. 16: Trace element abundance in sulfides minerals. Au, As, Sb and Ag.

Other trace elements

Se and Te have a strong correlation ($r=0.97$). Se and Te are enriched in pyrite and arsenopyrite. Se shows concentration ranges and mean values in pyrite and arsenopyrite of respectively 4.40ppm -

37.70ppm, 9.40 ± 1.78 ppm (n=18) and 23.96ppm – 26.87ppm, 25.42 ± 1.45 pm (n=2). Pyrite and Arsenopyrite exhibits Te concentration ranges and mean of respectively 0.17ppm – 24.98ppm, 3.46 ± 1.50 ppm (n=18) and 34.15ppm – 36.66ppm, 35.41 ± 1.25 ppm (n=2). Se has peak value in pyrite of 37.70ppm (n=18) and Te has peak value in arsenopyrite with a value of 36.66ppm (n=2). Se and Te enrichment in both pyrite and arsenopyrite correspond to Au peaks (Fig. 17). Hg has in general a low concentration with a peak value of 16.4ppm in sphalerite (Fig. 17) and a mean value of 1.08 ± 0.69 ppm (n=25). Hg has a strong correlation with W ($r=0.99$). Galena is the main carrier for Ag (Fig. 16), all other sulfides exhibits low Ag concentration albeit cobaltite and chalcopyrite have higher Ag concentration relative to the rest of the sulfides. Ag shows a strong correlation with Pb ($r=0.64$). Sphalerite has Ag peak value of 7282ppm and mean value of 1561 ± 826 ppm (n=8). Bi has a peak value in pyrite of 57.63ppm and but values are in general fairly low. Bi was measured only in pyrite and arsenopyrite. The main host for Cu is chalcopyrite with concentration ranging and mean values of respectively 21.90% to 35.37% and 32.56 ± 7.71 % (n=16), though cobaltite shows an enrichment with peak value and mean of respectively 32.11% and 4.99 ± 3.92 % (n=8).

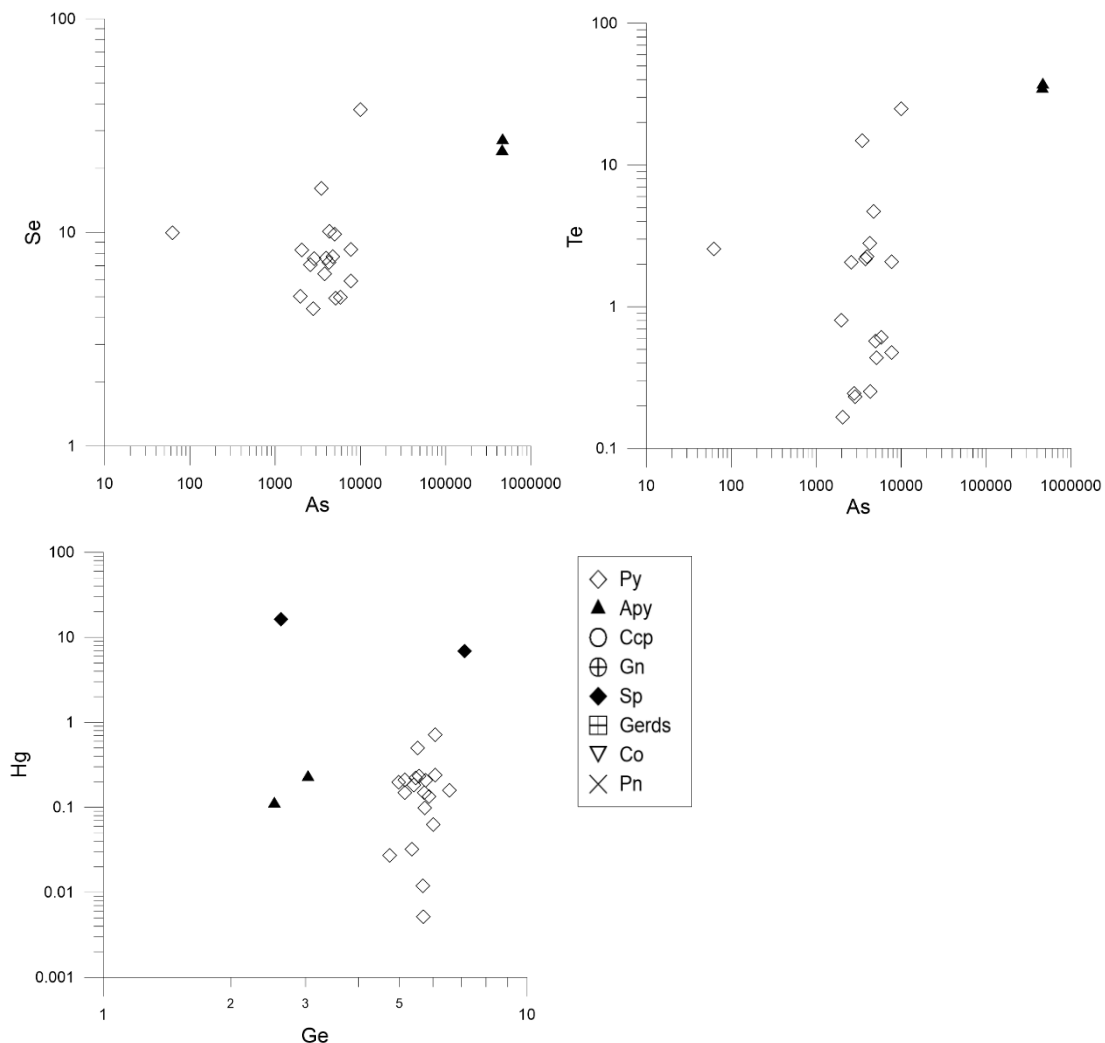


Fig. 17: Trace element abundance in sulfides minerals. Se, Te and Hg.

7. Discussion

7a. Protolith composition

The choice of unaltered samples was made based on both the absence/presence of alteration minerals such as sericite or ankerite, the state of preservation of sedimentary features and also the estimated extent of hydrothermal alteration in the host rock. The 25 samples selected have none or the least alteration minerals content visible in thin section and sedimentary textures fairly well preserved. During the sampling of the background samples care was taken to avoid sampling near the multiple late doleritic intrusions that are present in the host rock, the late veins that cross cut the sequence, fault gouges and breccias to avoid the influence of late variation not directly related to the hydrothermal system and the subsequent mineralisation.

Given that the host rock has different composition, it is critical to eliminate the primary variation in element concentration caused by host rock variation in order to accurately constrain mass change. The protolith composition and the distribution of metal contents in the protolith was determined using differentiation curves following the method of Jowitt et al. (2012). The method suggests that the protolith composition of a given suite of samples define a differentiation curve in a binary plot (XY) and that the regression coefficients of the differentiation curve remain constant during rock formation; a least square regression line in a form of a power law curve should reproduce the variation of the concentration of elements forming the rock at differing concentration of an immobile and incompatible element.

$$\text{Equation (1): } E_e = A I^B$$

Where E_e is the estimated element concentration for a given immobile element concentration (I), A and B are regression coefficients. The background variation in protolith samples relative to the differentiation model (regression line) was quantified by determining either the Root Mean Square of Deviations (RMSD) between the model and the data (Equation 2), for elements showing a moderate to strong correlation with the chosen immobile elements, either by using the median concentration of the element concentration as a baseline (model) and the 1st and 3rd quartiles as measure of background variation for the element under investigation. Statistical analysis of the correlation was performed to determine the correlation coefficient and their statistical significance in order to decide whether to use the differentiation regression curve as model and the RMSD or Median as model and the quartiles to investigate the background variation of different elements.

$$\text{Equation (2): } RMSD = \sqrt{\frac{\sum(E_e - E_m)^2}{n}}$$

Where E_e is the calculated element concentration at the measured concentration of the immobile element " I " from Eq. (1), E_m is the measured element concentration in the protolith sample and n is the number of samples used to define the model.

Isochon diagrams (Fig. 18) based on the average geochemical composition of the 2 different lithologies (least altered samples) amongst the 25 unaltered samples and the ore sample (most altered sample), show that TiO_2 , P_2O_5 and most REE were fairly immobile during hydrothermal

alteration of the rock sequence. Although being generally an immobile element during alteration and metasomatism, Al_2O_3 appears to have been partially mobilised during alteration at the Blackwater deposit, Therefore TiO_2 was used as an immobile element for our protolith composition calculation using equation 1 as follow:

$$\text{Equation (2): } E_e = A * (TiO_2)^B$$

Where E_e is the estimated element concentration for a given TiO_2 concentration (TiO_2), A and B are regression coefficients (ESM 5). Correlation coefficient (Table 5) were determine by plotting in a binary plot the element under investigation against TiO_2 . The strength of the correlation coefficients were assessed for their statistical significance using the non-parametric test of Spearman to determine the Spearman correlation coefficient and the p-values at $\alpha < 0.01$ in order to decide whether

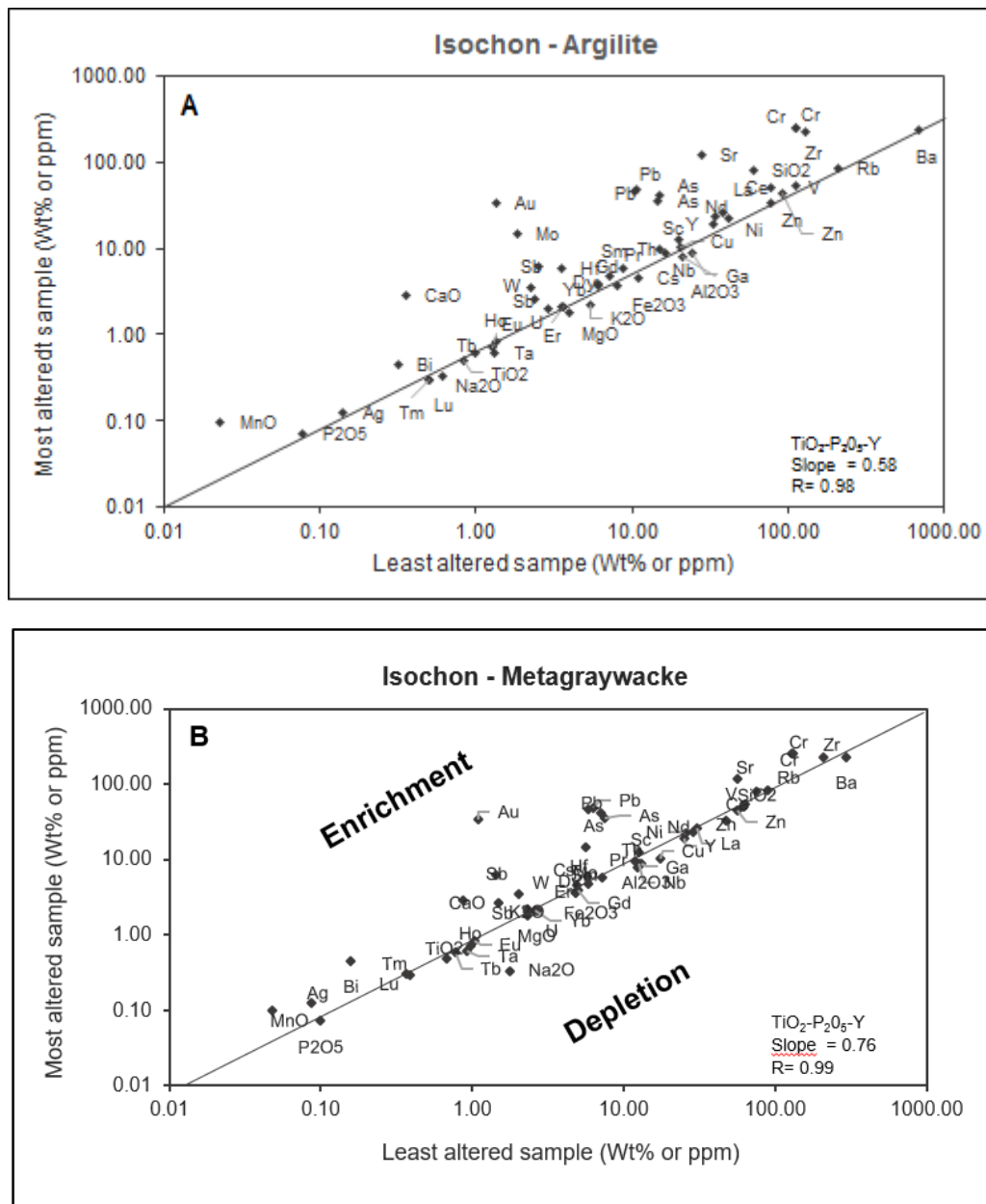


Fig. 18: Isochon diagrams showing immobile elements and elements that have undergone gain or loss during alteration. The concentration from least altered rock are plotted against ore or most altered samples. A) Argillite. B) Metagraywacke.

to use the regression line to calculate E_e or use the median value as a model of background variation. As a rule of thumb the following guide was used to describe the strength of the Spearman correlation coefficient " r_s ":

If r_s has a value between,

$\pm 0.00-0.19$ "very weak", thus $p \gg 0.0001$, use median value as E_e

$\pm 0.20-0.39$ "weak", thus $p > 0.0001$, use median value as E_e

$\pm 0.40-.59$ "moderate", thus $p < 0.0001$ or $p \sim 0.0001$, use differentiation curve to estimate E_e

$\pm 0.60-.79$ "strong", thus $p << 0.0001$, use differentiation curve to estimate E_e

$\pm 0.80-1.0$ "very strong", thus $p << 0.0001$, use differentiation curve to estimate E_e

The exception to these rules was made when the differentiation curves and the RMSD did not capture consistently the variation of the background concentration of the elements under investigation. In that case median value was used as E_e . The r_s and p-values for the 25 unaltered samples are reported in table 6.

7b. Mass balance

The mass balance calculation is appropriate if there has been at least one element that stayed immobile during hydrothermal alteration. Large decrease or increase of mass during alteration can result in residual concentration or dilution. Isochon diagrams indicated that Ti has been relatively immobile during alteration at Blackwater, thus Ti constitutes an appropriate proxy to investigate the mass balance of various elements of interest related to Au mineralisation in the Blackwater core. The method described by Jowitt et al (2012) was used to perform mass balance calculation. The % of change in the element of interest is estimated by:

$$\% \Delta e = (E_m - E_e) / E_e * 100$$

Where E_e is the estimated concentration of the element under investigation obtained either through the differentiation curve equations or using the median value as a baseline for element showing very weak and weak correlation with Ti and E_m is the measured value in our sample. $\% \Delta e$ is the %change (enrichment or depletion) in the element of interest e. This method provides a better estimate of our estimation of the amount of metals and elements of interest mobilised during hydrothermal alteration because modelling the protolith concentration for each individual sample using the differentiation curves increases the accuracy of our protolith composition rather than selecting an "average" protolith.

Gold (Au)

Au concentration in the protolith varies from 0.37ppb to 30.45ppb. The high variation up to 30ppb is probably the result of nugget effect in the gold distribution because the sulfides to which they are associated with are not homogeneously distributed through the sequence of metasedimentary rocks forming the host rock. The mean and median are respectively 2.92ppb and 0.97ppb.

Given the weak correlation and p-values (Table 6) for Au vs Ti, the background variation of Au in the protolith was calculated using the median Au value as a baseline and the 1st and 3rd quartiles.

Distal alteration

Au concentrations in the distal alteration sample suite varies between 0.86ppb and 6.38ppb. The mean and the median values are respectively 1.92ppb and 1.25ppb. The enrichment of Au or mass change (% Δ Au) in the distal alteration halo varies from -11% to 559% with mean and median values of 98% and 57%. The enrichment shows a systematic increase in % Δ Au in the argillite unit while in the greywacke the increase is irregular (Fig. 19).

Proximal alteration

The proximal alteration halo has Au value ranging from 0.62ppb to 28.65ppb. The % Δ Au in the proximal alteration halo changes from -35% to 2895%. The mean and median values are respectively 551% and 113%. The %Au enrichment in the distal and proximal alteration define an Au alteration halo of about 40 meters comprising 20 meters above the quartz lodes and 20 meters below the quartz lodes (Fig. 19). The ore has an Au concentration of 66.99ppb which represents a % Δ Au of 6806%.

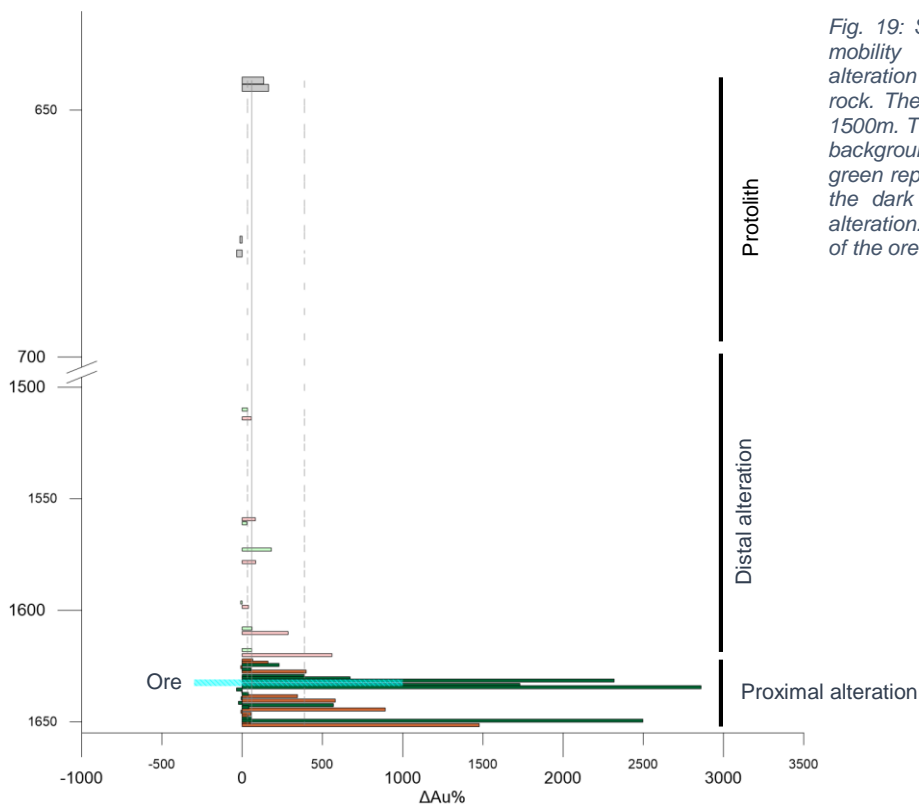


Fig. 19: Strip log illustrating the % Δ Au mobility in the distal and proximal alteration relative to the unaltered host rock. The Y axis is broken from 700 to 1500m. The 2 dotted lines represent the background variation. The light red and green represent the distal alteration and the dark red and green the proximal alteration. The cyan bar is the location of the ore bearing quartz lode.

Arsenic (As)

As concentration in the protolith range between 2.68ppm and 30.08ppm and the mean and median are respectively 14.18ppm and 13.41ppm. The correlation between As and the immobile element Ti is very weak (Table 6), and the background variation of As in the protolith was calculated using the median As value as a baseline and the 1st and 3rd quartiles.

Distal alteration

As concentration in the distal samples suite varies between 5.03ppm and 93.18ppm. The mean and the median values are respectively 17.73ppm and 110ppm. The % Δ As in the distal alteration halo varies from -62% to 594% with mean and median values of 98% and 57% (Fig. 20).

Proximal alteration

As values in the proximal alteration halo range from 8.62ppm to 94.67ppm. The % Δ As changes from -35% to 605%. The mean and median values are respectively 203% and 188%. As alteration halo relative to the distal and proximal alteration is ~45 meters containing 22 meters above the quartz lodes and 23 meters below the quartz lodes and most likely extend further down since the last proximal sample still indicate a significantly high As concentration (Fig. 20). As has a very weak correlation with Au, which indicates that it behaves differently during hydrothermal alteration at Reefton. Although both are enriched in the ore bearing quartz lodes, their enrichment does not occur in the same way.

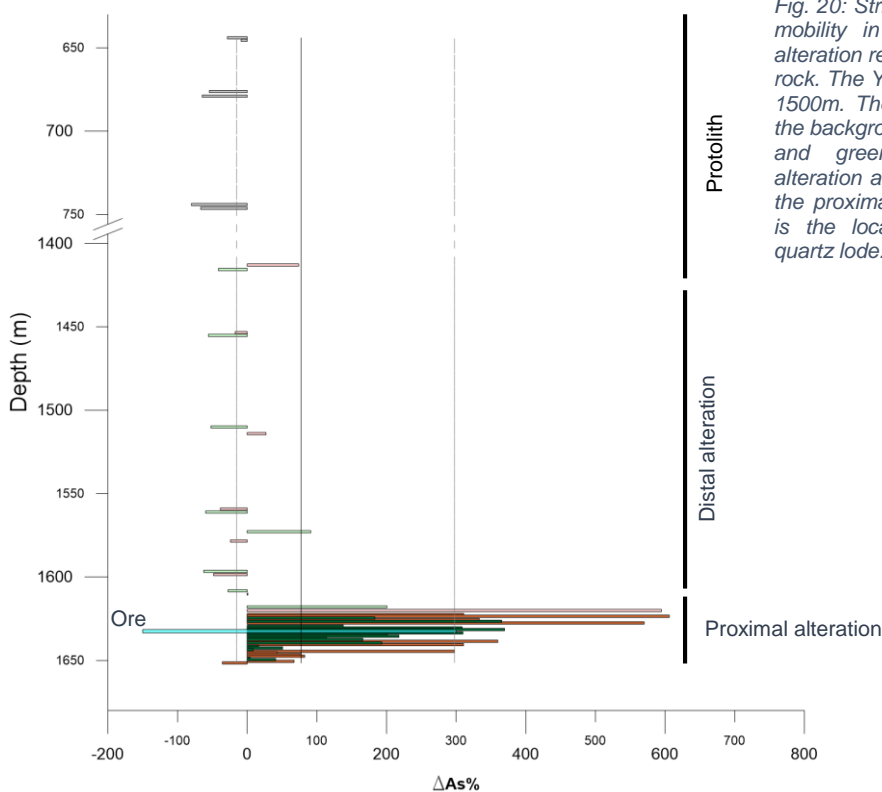


Fig. 20: Strip log illustrating the % Δ As mobility in the distal and proximal alteration relative to the unaltered host rock. The Y axis is broken from 700 to 1500m. The 2 dotted lines represent the background variation. The light red and green represent the distal alteration and the dark red and green the proximal alteration. The cyan bar is the location of the ore bearing quartz lode.

Antimony (Sb)

Antimony has a fairly low range of concentration variation in the background it varies 0.15ppm to 4.46ppm. The mean and median are 2.04ppm and 2.00ppm respectively. The background variation of Sb in the protolith was calculated by means of the median Sb value as a baseline and the 1st and 3rd quartiles.

Sample#	JH07831	JH07830	JH07829	JH07826	JH07825	JH07822	JH07823	JH07821	JH07819	JH07818	JH07817	JH07815	JH07814	JH07811	JH07806	JH07807	JH07998	JH07997
Lithology	G	A	G	G	A	A	G	A	A	G	A	A	G	G	A	A	A	G
Depth (m)	644	645.5	676.2	746.2	795	843.3	844.1	900.8	945.9	949.6	996.4	1045.3	1047.7	1143.8	1243.7	1242.9	1293.75	1299.4
Distance from quartz lode	988.5	987	956.3	886.3	837.5	789.2	788.4	731.7	686.6	682.9	636.1	587.2	584.8	488.7	388.8	389.6	338.75	333.1
SiO2	74.85	58.34	72.46	76.34	56.77	56.66	77.15	62.70	65.74	75.49	62.70	59.36	71.51	73.57	57.34	67.10	62.11	72.09
Al2O3	12.08	21.82	13.85	10.18	22.07	22.93	11.44	19.20	17.45	11.52	18.47	21.21	14.11	13.20	22.08	16.12	19.32	11.24
Na2O	1.84	0.44	1.79	1.44	0.49	0.36	1.44	0.81	1.11	1.38	1.11	0.70	1.49	1.83	0.57	1.24	1.01	1.84
K2O	2.14	5.79	2.70	2.10	5.57	6.26	2.18	4.82	3.94	2.65	4.28	5.63	2.96	2.47	5.76	3.66	4.73	2.42
TiO2	0.65	0.80	0.73	0.53	0.78	0.86	0.64	0.75	0.83	0.63	0.79	0.75	0.73	0.68	0.82	0.78	0.76	0.61
LOI@550	2.97	4.55	3.01	5.41	4.58	2.58	4.50	4.27	3.62	4.55	4.47	1.93	1.47	1.37	11.96	1.82	4.05	7.37
Au	2.27	2.56	0.83	0.75	0.41	3.50	1.51	0.54	0.87	30.45	4.37	1.51	0.59	0.37	8.07	3.88	2.62	2.26
As	9.59	12.25	6.13	4.45	30.08	5.90	13.58	18.59	14.52	18.12	17.95	19.60	11.88	10.73	23.00	19.22	20.81	13.41
Sb	1.79	3.33	1.35	1.25	2.13	1.76	2.88	2.03	2.04	0.15	2.21	2.95	2.00	1.50	4.46	2.55	3.18	1.42
Cr	126.97	107.23	120.00	162.00	106.67	109.60	147.33	99.37	129.30	150.20	94.57	108.93	122.47	113.23	95.83	128.60	80.80	47.53
Ni	25.68	45.20	28.11	19.46	45.97	45.43	23.06	37.40	37.70	19.68	37.87	47.87	29.43	26.99	43.90	32.20	37.50	18.64
Cu	25.26	40.13	11.34	12.89	4.06	41.53	11.62	17.03	24.67	15.24	42.07	25.07	19.32	16.59	25.27	33.43	26.03	15.57
Zn	42.87	76.33	46.70	39.60	66.10	74.90	37.57	70.30	84.77	51.20	67.03	104.67	73.27	51.13	61.00	53.93	62.87	44.60
Rb	80.60	222.07	102.93	81.20	226.67	251.73	87.50	193.53	153.83	103.10	164.57	225.47	124.30	96.83	267.73	146.50	180.47	93.17
Sr	56.53	22.79	44.23	91.03	28.07	21.08	36.03	34.30	32.83	103.70	42.73	22.84	57.87	38.83	21.09	62.50	31.91	222.27
Mo	5.37	1.71	4.59	8.18	0.83	0.67	6.58	1.15	4.22	6.96	1.39	1.39	4.39	4.11	1.15	4.15	0.32	0.29
W	1.89	1.91	1.98	2.04	2.21	2.19	2.14	2.12	2.56	2.13	2.44	2.08	2.21	2.15	20.39	2.88	25.26	108.90
Pb	9.32	6.32	5.17	30.26	2.57	2.55	3.81	8.11	11.27	16.12	4.28	9.18	25.83	5.99	18.66	8.12	15.29	18.02
Bi	0.28	0.61	0.13	0.20	0.15	0.80	0.11	0.61	0.17	0.20	0.18	0.17	0.36	0.32	0.87	0.25	0.86	0.26

Table 4 : Geochemical composition of some of the 25 unaltered samples used to determine protolith composition and background variation of the concentration of selected elements of interest. **G**: Metagraywacke; **A**: Argillite.

Distal alteration

The Sb content in the distal alteration zone varies from 1.37ppm to 14.47ppm, the profile downhole is fairly monotonous until the lower section of the distal alteration where a gradual increase is observed. The % Δ Sb range from -31% to 623% with mean and median values of respectively 81% and 31% (Fig. 21).

Proximal alteration

Sb concentration in the proximal alteration halo varies from 4.42ppm to 19.83ppm. The % Δ Sb ranges from 121% to 891%. The mean and median values are respectively 389% and 327%. Sb alteration halo relative to the distal and proximal alteration is about 40 meters including 20 meters above the quartz lodes and 20 meters below the quartz lodes (Fig. 21). Sb concentration has a strong correlation with As, which indicate that they behave similarly during hydrothermal alteration at Reefton.

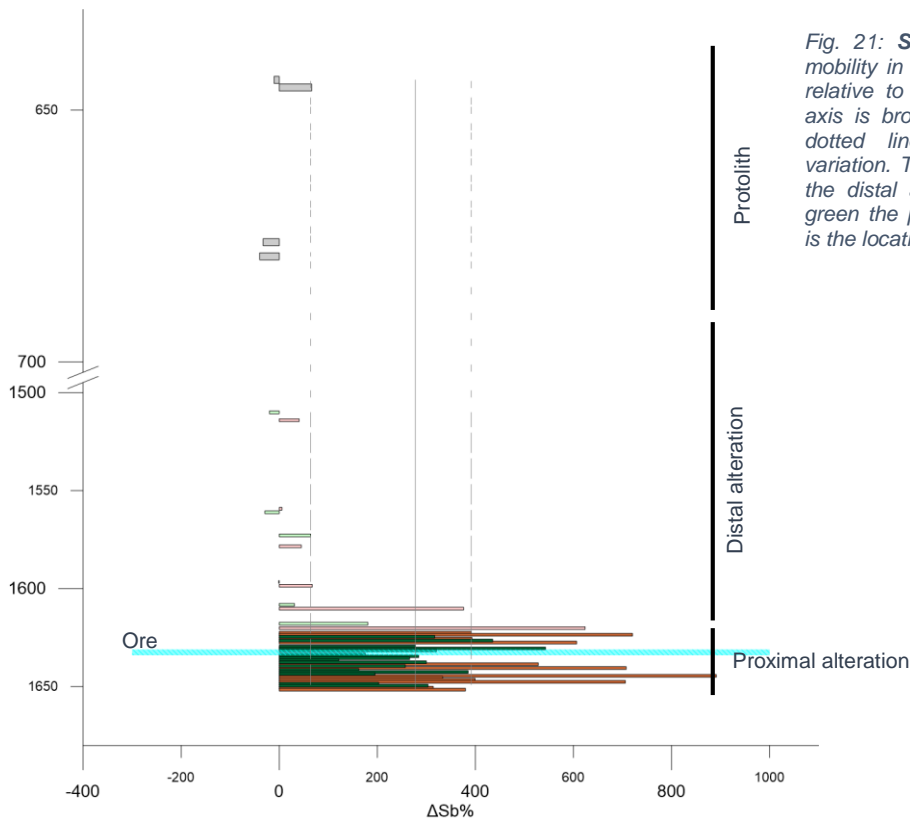


Fig. 21: Strip log illustrating the % Δ Sb mobility in the distal and proximal alteration relative to the unaltered host rock. The Y axis is broken from 700 to 1500m. The 2 dotted lines represent the background variation. The light red and green represent the distal alteration and the dark red and green the proximal alteration. The cyan bar is the location of the ore bearing quartz lode.

Potassium (K₂O) and sodium (Na₂O)

Background concentrations of Na₂O and K₂O have range of 0.36wt% to 1.84wt% and 1.80wt% to 6.26wt% respectively. Their mean and median are respectively 1.20wt% and 1.32wt% for Na₂O and 3.74wt% and 3.66wt% for K₂O. The background variation for K₂O and Na₂O were estimated using the regression lines and RMSD.

Distal alteration

The % Δ K₂O and % Δ Na₂O commonly display antipathetic trend where enrichment of K₂O corresponds to Na₂O depletion and vice versa. The value corresponding to minimum and maximum corresponding values of % Δ K₂O are -51% and 54% Δ Na₂O changes between -98% and 126% (Fig. 22).

	Au	As	Sb	Cr	Ni	Cu	Zn	Rb	Sr	Mo	W	Pb	Bi	SiO2	Al2O3	Na2O	K2O	TiO2	LOI	
Au	1.00																			
As	0.10	1.00																		
Sb	0.10	0.77	1.00																	
Cr	0.73	0.03	0.02	1.00																
Ni	-0.32	0.39	0.33	-0.33	1.00															
Cu	-0.11	0.18	0.33	-0.27	0.57	1.00														
Zn	-0.19	0.43	0.43	-0.20	0.67	0.40	1.00													
Rb	-0.20	0.43	0.42	-0.31	0.75	0.42	0.56	1.00												
Sr	0.10	0.02	0.08	-0.05	-0.53	-0.20	-0.39	-0.23	1.00											
Mo	0.73	-0.06	-0.05	0.96	-0.55	-0.36	-0.35	-0.48	0.12	1.00										
W	0.29	0.47	0.28	0.17	-0.02	-0.08	0.04	0.14	0.22	0.16	1.00									
Pb	0.52	0.22	0.36	0.41	-0.07	0.16	0.09	0.00	-0.01	0.38	0.12	1.00								
Bi	0.33	0.12	0.28	0.17	0.30	0.44	0.24	0.27	-0.31	0.08	-0.08	0.72	1.00							
SiO2	0.38	-0.33	-0.32	0.51	-0.88	-0.53	-0.61	-0.92	0.31	0.68	0.01	0.12	-0.24	1.00						
Al2O3	-0.37	0.27	0.29	-0.47	0.87	0.49	0.61	0.93	-0.41	-0.65	-0.03	-0.12	0.26	-0.98	1.00					
Na2O	-0.39	-0.57	-0.49	-0.30	-0.39	-0.17	-0.33	-0.66	0.11	-0.15	-0.51	-0.29	-0.30	0.43	-0.44	1.00				
K2O	-0.19	0.52	0.50	-0.31	0.78	0.44	0.61	0.98	-0.24	-0.48	0.14	0.02	0.26	-0.92	0.92	-0.68	1.00			
TiO2	-0.55	0.26	0.29	-0.67	0.71	0.41	0.53	0.73	-0.21	-0.78	0.03	-0.33	-0.04	-0.83	0.83	-0.18	0.74	1.00		
LOI	-0.13	0.48	0.25	-0.18	0.32	0.12	0.37	0.34	-0.19	-0.25	0.43	-0.03	-0.02	-0.32	0.30	-0.26	0.37	0.26	1.00	

Table 5. Correlation coefficient for selected elements in the unaltered sequence.

Elements	Spearman r_s	p-values > p	TiO2	Cu	0.4719	<.0001	TiO2	Pb	0.0367	0.7595
TiO2 Au	0.1349	0.2586	TiO2 Zn	0.674	<.0001	TiO2 Bi	0.4168	0.0003		
TiO2 As	0.2134	0.0719	TiO2 Rb	0.7986	<.0001	TiO2 SiO2	-0.8254	<.0001		
TiO2 Sb	0.3881	0.0008	TiO2 Sr	-0.5068	<.0001	TiO2 Al2O3	0.8521	<.0001		
TiO2 Cr	-0.3232	0.0056	TiO2 Mo	-0.4876	<.0001	TiO2 Na2O	-0.4286	0.0002		
TiO2 Ni	0.7564	<.0001	TiO2 W	0.2082	0.1425	TiO2 K2O	0.8238	<.0001		

Table 6: Spearman rank correlation coefficient and p-values for selected elements. The analysis was carried out with a $\alpha=0.01$

Proximal alteration

K₂O and Na₂O concentrations proximal to the Au quartz vein vary from 2.33wt% to 7.58wt% and 0.02wt% to 1.68wt% respectively. Both the mean and median values for K₂O are 0.73wt% and the corresponding value for Na₂O are 0.93wt% and 0.92wt%. %ΔK₂O and %ΔNa₂O changes respectively from 43% to 113% and 73% to -234%. K₂O and Na₂O appears to form an alteration halo around the main Au quartz vein of about 40 meters and this halo fairly correlate with Au and other pathfinder elements (Sb and As).

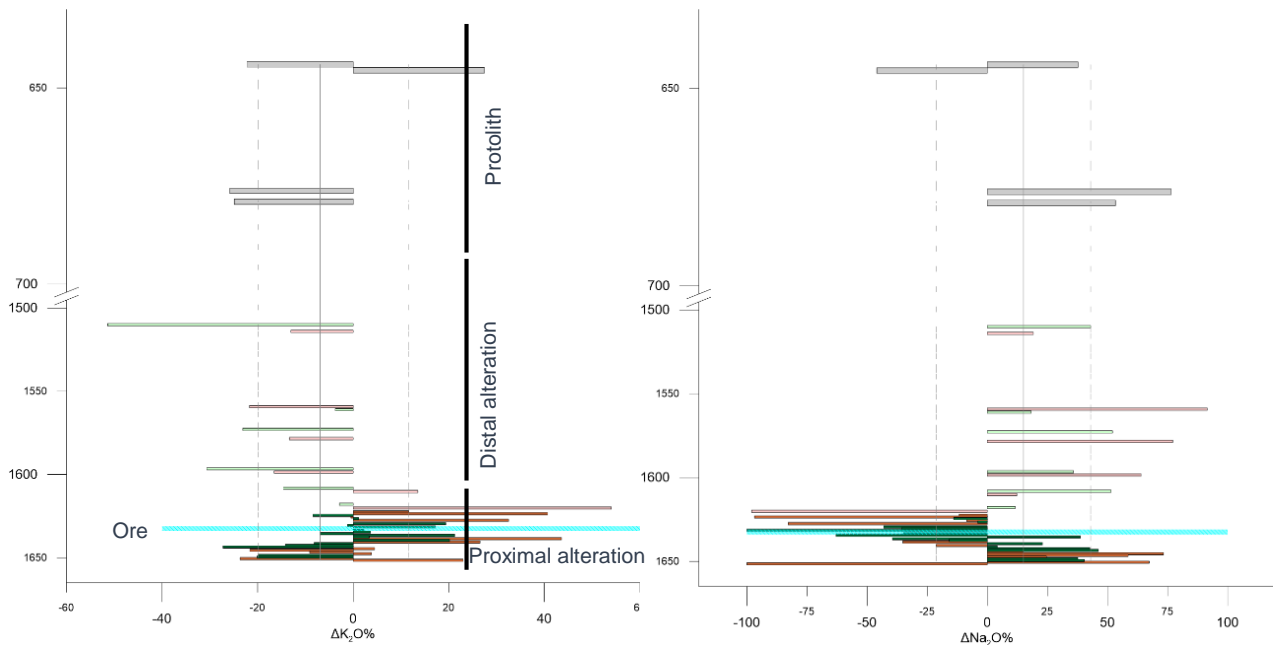


Fig. 22: Strip log illustrating the K₂O (A) and Na₂O (B) mobility in the distal and proximal alteration relative to the unaltered host rock. The Y axis is broken from 700 to 1500m. The 2 dotted lines represent the background variation. The light red and green represent the distal alteration and the dark red and green the proximal alteration. The cyan bar is the location of the ore bearing quartz lode.

7c. Hydrothermal alteration

The style of hydrothermal alteration and mineralisation at Blackwater is similar to other orogenic gold deposits described at Reefton (Christie & Brathwaite 2003). Hydrothermal alteration at Blackwater is marked by formation of hydrothermal minerals, recrystallisation of metamorphic minerals and replacement of minerals formed prior alteration.

Some of these mineralogical changes are subtle because some minerals present in the pre-alteration assemblage are also formed during hydrothermal alteration. The variation in concentration of major oxides relative to the lithology (sandstone, siltstone or mudstone) makes it difficult to define the alteration halo using geochemical plot from single major oxides elements. Because the argillite for example will have high Al₂O₃ and K₂O and the metagraywacke will have significantly high SiO₂ compared to the argillite unit.

However, several alteration indexes in the forms of molar ratios of major oxides have been developed and successfully applied to overcome the issues above mentioned and investigate the magnitude and

extent of hydrothermal alteration halo in the wall rock of orogenic gold deposits (Eilu & Mikucki 1998; Eilu & Groves 2001). (Eilu & Mikucki 1998; Eilu & Groves 2001). Alteration indexes can be define by the formula (Ishikawa et al. 1976; Large et al. 2001):

$$\text{Alteration index} = \frac{\text{Element(s)enriched}}{\text{Element(s)enriched} + \text{Element (s)depleted}} \times 100 \text{ (if value in \%)}$$

In the sample suite collected the usage of the trends of Fe₂O₃, MgO and CaO to define the extent of hydrothermal alteration is difficult because their background variation does not show significant changes compared to the distal and proximal zones and the changes in the distal and proximal zones are rather erratic. However elements such as NaO, K₂O and LOI (CO₂) exhibits enrichment and depletion patterns that are most likely the result of hydrothermal alteration. Other elements which are mobile during hydrothermal alteration such as Ba, Sr and Rb shows high concentration proximal to the ore but their enrichment/depletion pattern appears to be erratic.

The potassic alteration index using molar ratios 3K/Al and sodic alteration index Na/Al represent the K-mica and albite respectively. A value of 1 for the Na/Al suggest that all the Na available in the sample is contained by Albite (Eilu & Mikucki 1998). The albite index has a monotonous trends in the protolith, distal up to the proximal alteration but sharply decrease ~20 meters away from the Birthday reef and gradually increase in and below the Birthday reef (Fig. 23). The K-mica index has an opposite trends compare to the albite index, there is a sudden increase near the ore and the peak value is also in the ore. The opposed behaviour of both alkali index reflect the replacement of albite by K-mica (muscovite or sericite) and/or carbonate. The distal alteration is marked by albite and the proximal is marked by a significant increase in sericite and muscovite.

The chlorite index (CI) is define by (Fe₂O₃+MgO)/(Fe₂O₃+MgO+CaO+Na₂O). The CI has profile is erratic although there seems to be a relatively fair drop in of values near the birthday reef (Fig. 23). This drop in values may correspond to the uptake of Fe and Mg in Fe-Mg carbonates formed during hydrothermal alteration. Metamorphic chlorite (pre-alteration) seems to be present in the entire core and therefore is most likely obscuring the signal of hydrothermal chlorite.

The loss on ignition at 105°C (LOI₁₀₅) and at 550°C (LOI₅₅₀) were used to determine the water content and the CO₂ content respectively following the methods defined by Dean (1974). Given that the amount of CO₂ that can be added to a rock undergoing alteration is largely controlled by Fe, Mg and Ca content in the unaltered rocks, the carbonation index CO₂/Ca+Mg+Fe has been developed to measure the degree of carbonate saturation by Fe, Mg and Mg-bearing minerals (Christie & Brathwaite 2003). This carbonation index increase significantly from values of 0.2. to 0.8 at ~20 meters above the main Au quartz vein, though the values also fall abruptly in the main Au vein. This increase indicates the intake of CO₂ in newly formed carbonates minerals. In hand specimens, carbonate alteration is easily observable in the lower section of the distal samples suite and in the proximal samples suite to the main Au quartz vein where there is commonly carbonates spotting, veining and disseminated carbonates grains in the matrix.

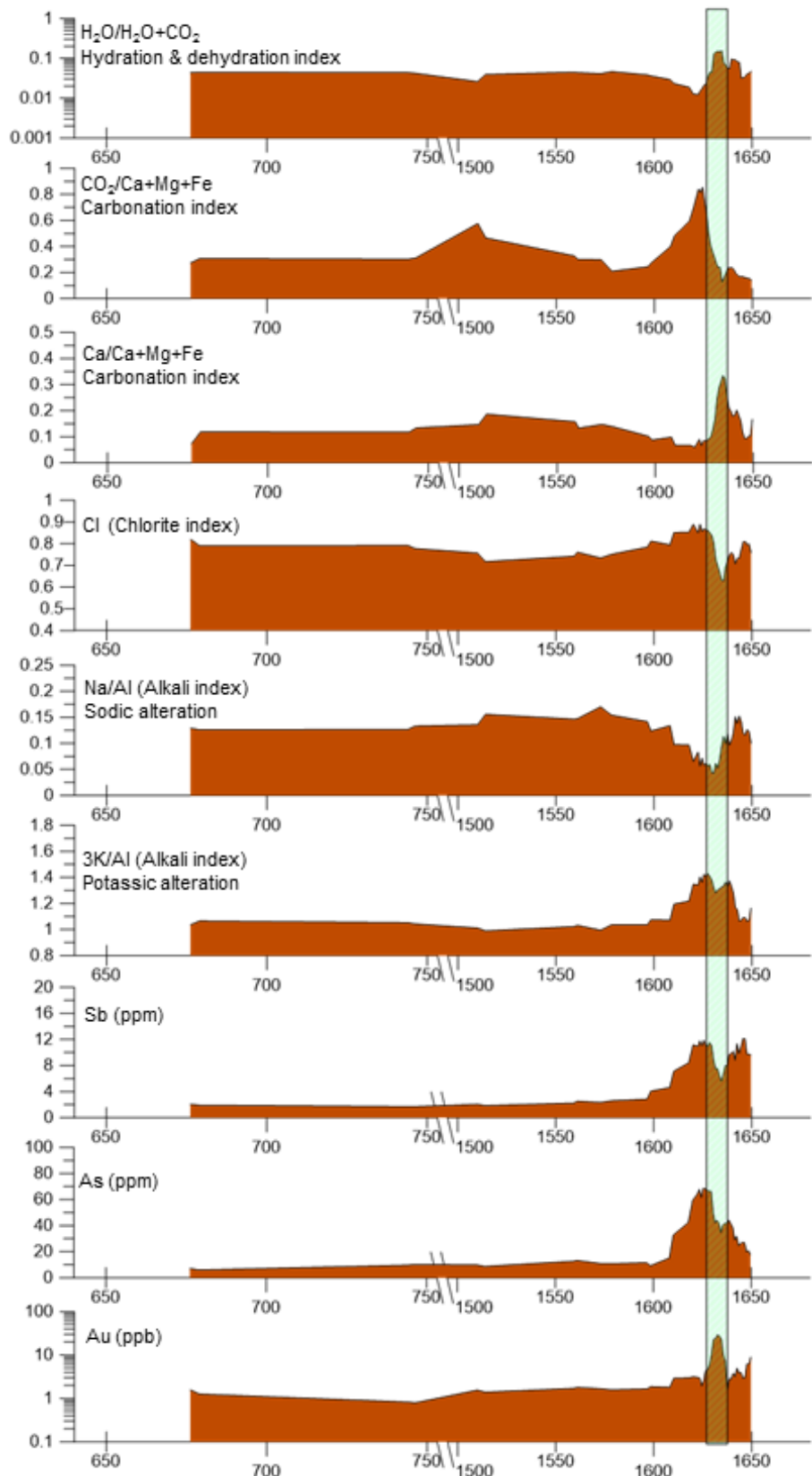


Fig. 23: Profiles showing weighed average of Au, As, Sb and alteration index footprint.

According to Kishida & Kerrich (1987) the bivalent cations Fe, Mg, and Ca are silicates hosted in unaltered rocks but as carbonation proceeds, the cations are progressively transferred to carbonate minerals and the above carbonation index approach the value of 1 which is the saturation value. The binary plot (Fig. 14) Ca/Ti vs. CO₂/Ti indicates that almost all the samples plot in the ankerite and dolomite and magnesite-siderite field. The same observation has been made for other deposit in the Reefton Goldfield highlighting the scarcity of calcite compared to ankerite-dolomite and ferroan magnesite-magnesian siderite in the hydrothermal assemblages at Reefton (Christie & Brathwaite 2003).

The carbonation index Ca/(Ca+Mg+Fe) has a noticeable increase proximal to the Birthday reef similar to the Au enrichment halo and a gradual decrease below the reef (Fig. 23). Carbonation indexes at Blackwater are to be used with caution for the reason that there are carbonates veining phases that are late during the mineralisation process and they may influence the carbonation index profile.

The index H₂O/(H₂O+CO₂) accounts for hydration and/or dehydration during hydrothermal alteration. Its profile in the distal to proximal alteration is rather monotonous but there is a sharp increase ~10 meters above the main Au veins similar Au, As and Sb profiles (Fig. 23).

7d. Mineral control on mass change

The down hole profiles of Au, As and Sb indicate increasing concentrations near the Au bearing quartz vein. The mass change %ΔAu, %ΔAs and %ΔSb values indicate an enrichment in Au, As and Sb of 6806%, 605% and 891% respectively relative to concentrations in the protolith. These chemical change are assumed to be the result of changes in the mineralogy due to hydrothermal alteration proximal to the Au quartz vein.

The abundances of Au, As and Sb bearing sulfides (arsenopyrite, pyrite, cobaltite, gersdorffite and ullmannite for the ore zone) increase towards the ore. Arsenopyrite and pyrite are the main Au-bearing minerals in the proximal and ore zone. Cobaltite, gersdorffite, ullmannite and to a lesser extent pyrite are the main As/Sb-bearing minerals in the distal and proximal alteration zones, in addition to arsenopyrite in the ore zone. SEM scans and *in-situ* LA-ICPMS analyses indicate that Au mineralisation is associated with pyrite and arsenopyrite either as free Au (electrum) or Au within pyrite and arsenopyrite where the Au is controlled by lattice substitution or micro/nano inclusions detectable with *in-situ*-LA-ICPMS analysis. Arsenic does not correlate strongly with Au in whole rock analyses, most likely because As sits in minerals other than pyrite and arsenopyrite such as chalcopyrite, cobaltite and gersdorffite which are not necessarily enriched in Au.

Other trace elements such as Ni, Cu and Co appear to have been mobilised during hydrothermal alteration however this process was most likely local as indicated by the mass balance (ESM 8c) that shows no systematic mobility for these elements. Furthermore their profile downhole is rather erratic and no reliable halo can be defined (ESM 3).

Textural relationships in thin section also suggest replacement relationships involving ullmannite, pentlandite and sphalerite that may also result in local remobilisation of Ni, Cu, Zn, Co but not enough in-situ LA-ICPMS data are available for these minerals due to grain size smaller than the beam size.

Ag and Pb are hosted mostly in galena and to a lesser extent in pyrite. Galena occurs mostly as inclusions and fracture fill in pyrite, indicating that the Ag and Pb enrichment may occur late in the Au mineralisation process.

The replacement of Na-plagioclase (albite) by K-mica (sericite/muscovite) due to hydrothermal reactions (Fig. 23) results in the sharp decrease in Na above the Au quartz lode and increase in K and reversal process below the Au quartz lodes. The enrichment/depletion in K & Na also occur at roughly the same place as the As and Sb halo.

The LOI values show significant changes proximal to the ore reflecting the variation in the amount of volatiles (H₂O, CO₂ and S). The proximal alteration zone shows higher values than the distal and least altered rocks. The mass change %ΔLOI pattern is almost identical to the %ΔK₂O pattern. The LOI profile rise sharply at ~20 meters above the main vein before dropping in the Au quartz vein and increase again below the vein. This augmentation in volatiles abundance is subsequent to replacement of albite by hydrothermal sericite and muscovite, carbonation and sulphidation in the proximal and ore zone (most altered rocks).

Unlike other orogenic gold deposits (MacKenzie & Craw 2007) characterised by an increase in Mg proximal to the ore due to abundance of Mg-chlorite near Au-bearing quartz vein there is no consistent Mg increase proximal and towards the main Au vein. The reason may be that Mg abundance is diluted and decrease with addition of SiO₂ indicating declining amount of matrix during silicification and quartz-vein formation.

7e. Ore deposit footprint

The Birthday reef at Blackwater is hosted in an alternating sequence of metagraywacke and argillite of the Greenland group metamorphosed to lower greenschist facies. Mineralogical and geochemical analysis of the samples collected suggest that there is a clear alteration zone of approximately 40 meters enveloping the main Au quartz vein. This envelope or halo is geochemically distinctive from the rest of the wall rock. It is characterised by enrichment and/or depletion in several elements including Au, As, Sb, Na, K and LOI. The enrichment and depletion pattern constitutes the geochemical footprint of the Blackwater deposit at Reefton (Fig 24). Au, As and Sb increase gradually in the proximal alteration zone toward the ore. Na and K show antipathetic trend, Na decrease in the proximal zone while K increase. LOI also exhibits a distinctive increase towards the main Au quartz vein from the distal alteration zone.

Significant mineralogical changes distal to proximal to the birthday reef form a distinctive feature defining the mineralogical footprint and providing key gradient towards Au mineralisation. Characterisation of the wallrock alteration downhole provides a wider deposit footprint compared to geochemical indicators. Sericitisation of the wallrock intensifies distal to proximal to Au mineralisation and extend for ~50 meters around the Birthday reef. Chloritisation is most likely one of the most common alteration type present but presence of chlorite in the pre-alteration assemblages makes it difficult to define a consistent chlorite halo. Quartz-carbonates veins are common in the lower section of the distal alteration zone and increase in abundance towards proximal and Au mineralised zones extending for ~100 meters away from Birthday reef. Carbonates spots are frequent in the proximal zones and gradually increase toward Au mineralisation. The abundance of sulfides minerals including pyrite, arsenopyrite, cobaltite, gersdorffite, ullmannite, millerite and pentlandite is greater distal to proximal to Au mineralisation. Chemical analysis on sulfides indicates that the mineral changes controls the chemical variation in trace elements content.

The above mentioned features expands significantly the exploration target at Blackwater. Some of the features can directly be mapped in the field, such as carbonates spotting, chlorite alteration (to a certain extent since metamorphic chlorite is almost undistinguishable from hydrothermal chlorite in the field), bleaching appearance of the host rock, quartz-carbonates veining, and use as gradient for field exploration. Geochemical profiles of pathfinders' elements, enrichment and depletion patterns and other geochemical indicators provide key information enabling to vector from low Au anomaly distal to the ore zone to high Au anomaly proximal to the ore zone.

A schematic showing the mineralogical and geochemical footprint of Blackwater is presented below.

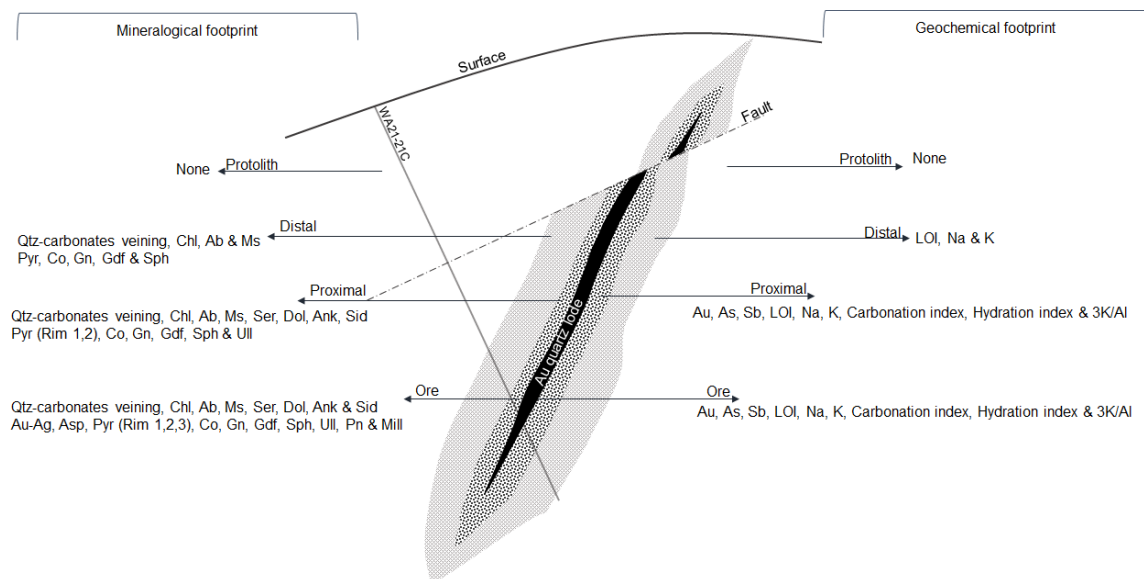


Fig. 24: Mineralogical and geochemical footprint of Blackwater Au deposit

8. Conclusions

Our investigation of wallrock alteration and its resulting geochemical changes at Blackwater provide new insights for the geochemical footprint of the main Au vein in the deposit, the Birthday reef. Geochemical analysis of Au, As and Sb using ultra-low detection limit reveals a clear geochemical footprint of about 20 meters above and below the birthday reef (40 meters in total), which is considerably larger than previous studies that reported an alteration halo of about 2 meters (Christie & Brathwaite 2003). This greatly increases the size of the geochemical anomaly that could be targeted during further exploration in the area. The clearest and largest elemental anomaly is seen in the Sb concentrations which indicate a consistent enrichment of Sb allowing to use Sb as a pathfinder element. Other elements such as Co, Ni, Cu and Zn show localised mobility but there is no evidence of significant enrichment that could be useful as a vector for exploration.

Mass variation in K_2O and Na_2O and the $3K/Al$ and Na/Al alkali alteration indexes show clear antipathetic trends reflecting the replacement of Albite by K-mica (sericite and muscovite). These trends provide one of the best geochemical indicators at Blackwater. $\% \Delta K_2O$ and $3K/Al$ increase with greater alteration intensity near the Birthday reef whereas $\% \Delta Na_2O$ and Na/Al decrease with alteration intensity. De-/hydration indices reflecting the volatile content (excluding S) although narrow can be used in combination with other alteration indices.

Bleaching of the wall rock, green chlorite alteration and carbonates spotting provide a clear field criteria than can be used for alteration mapping during early stage of exploration and can be combined at a later stage with carbonation and chlorite (except for Blackwater where chlorite is extensively part of the pre-alteration mineral assemblage) index. Other elements such as SiO_2 have been mobile during alteration as indicated by presence of quartz filling pressure shadow, but the mass change calculation shows that no significant SiO_2 addition has occurred.

Our results show that mineralogical and geochemical variations resulting from hydrothermal alteration of the wallrock in orogenic gold deposit cover a wider extent than Au mineralisation itself. These variations provide useful vectoring tools distal to proximal Au mineralisation at Blackwater. Because of the composite nature of wallrock alteration in orogenic gold deposits it is difficult to identify a single parameter characterising on its own both a consistent and significant vector to ore that extent far beyond the main ore vein into the host rock.

Therefore, it is important at least during early stage of exploration to identify key alteration type and once done define a broad vector towards advanced alteration zones. To reach this objective it is critical to start with a detailed alteration mapping then analyse a wide set of elements (including ultra-low detection analysis for Au and related elements – As, Sb, Te, Se, Ag, W, Mo, Bi,) and define the protolith composition and background variation. Following protolith characterisation, investigate elements mobility and select the most useful elements which are most likely the most mobile ones during alteration. Ensure

that the mobility is not local but rather broad and accompanied by enrichment/depletion at the deposit scale. Based on background variation, describe the extent and magnitude of the geochemical anomaly (footprint) to reveal the extent of the exploration target then follow up on the trend of geochemical vectors and alteration patterns (field based and alteration index) to vector from distal zone to proximal ore zone.

9. Electronic supplementary materials (ESM) Appendix

Electronic supplementary materials contain all analytical results, data analysis and figures produced for the writing of this thesis.

ESM 1 – Rock classification

ESM 2 – Whole rock geochemistry

ESM 3 – Au related elements downhole

ESM 4 – Spearman rank correlation coefficient and Correlation coefficient matrix

ESM 5 – Protolith composition

ESM 5a – Descriptive statistics protolith composition

ESM 5b – Differentiation curves

ESM 6 – Mass change calculation distal and proximal zones

ESM 6a – Descriptive statistics mass change distal and proximal zones

ESM 7 – Background variation – Protolith – LAICPMS

ESM 7a – Background variation – Protolith – XRF – Ultralow Au, As and Sb

ESM 8 – Mass balance – distal and proximal – LAICPMS

ESM 8a – Mass balance calculation distal proximal-XRF (selected elements) and Ultra-low Au, As and Sb

ESM-8b-Mass-balance-calculation-distal-proximal-XRF and Ultra-low Au, As and Sb

ESM-8c - Au related elements mass balance pattern downhole

ESM 9 – Alteration index

ESM 10 – *In situ* LA-ICPMS results

References

- Adams, C.J., Gabites, J.E., 1985. Age of metamorphism and uplift of the Haast Schist Group at Haast Pass, Lake Wanaka and Lake Hawea, South Island, New Zealand. *N.Z. J. Geol. Geophys.*, 28, pp.85–96.
- Adams, C.J. & Kelley, S., 1998. Provenance of Permian-Triassic and Ordovician metagraywacke terranes in New Zealand: Evidence from $^{40}\text{Ar}/^{39}\text{Ar}$ dating of detrital micas. *GSA Bulletin*, 110(4), pp.422–432.
- Adams, C.J.D., Harper, C.T. & Laird, M.G., 1975. K-Ar ages of low grade metasediments of the Greenland and Waitua Groups in Westland and Buller, New Zealand. *New Zealand Journal of Geology and Geophysics*, 18(1), pp.39–48.
- Ballance, P.F., Campbell, J.D., 1993. The Murihiku arc-related basin of New Zealand (Triassic–Jurassic) In: Ballance, P.F. (Ed.), *South Pacific Sedimentary Basins. Sedimentary Basins of the World 2, Elsevier, Amsterdam*, pp.21–33.
- Becker, J. a. et al., 2000. Gold mineralisation near the Main Divide, upper Wilberforce valley, Southern Alps, New Zealand. *New Zealand Journal of Geology and Geophysics*, 43(2), pp.199–215.
- Bierlein, F.P. et al., 1998. Wallrock alteration associated with turbidite-hosted gold deposits. Examples from the Palaeozoic Lachlan Fold Belt in central Victoria, Australia. *Ore Geology Reviews*, 13(1-5), pp.345–380.
- Bierlein, F.P., Christie, a. B. & Smith, P.K., 2004. A comparison of orogenic gold mineralisation in central Victoria (AUS), western South Island (NZ) and Nova Scotia (CAN): Implications for variations in the endowment of Palaeozoic metamorphic terrains. *Ore Geology Reviews*, 25(1-2), pp.125–168.
- Bierlein, F.P. & Maher, S., 2001. Orogenic disseminated gold in Phanerozoic fold belts - Examples from Victoria, Australia and elsewhere. *Ore Geology Reviews*, 18(1-2), pp.113–148.
- Bishop, D.G., Bradshaw, J.D., Landis, C.A., 1985. Provisional terrane map of South Island, New Zealand. In: Howell, D.G. (Ed.), *Tectonostratigraphic Terranes. Circum-Pacific Council for Energy and Mineral Resources, Houston, TX*, pp.515–521.
- Boiron, M.-C. et al., 1996. P-T-X conditions of late Hercynian fluid penetration and the origin of granite-hosted gold quartz veins in northwestern Iberia: A multidisciplinary study of fluid inclusions and their chemistry. *Geochimica et Cosmochimica Acta*, 60(1), pp.43–57.
- Bradshaw, J.D., Pankhurst, R.J., Weaver, S.D., Storey, B.C. & Muir, R.J., Ireland, T.R., 1997. New Zealand superterrane recognised in Marie Byrd Land and Thurston Island. In: Ricci, C.A. (Ed.), *The Antarctic Region: Geological Evolution and Process. Terra Antarctica Publication, Siena*, pp.429–436.
- Bradshaw, J., 1993. A review of the Median Tectonic Zone: terrane boundaries and terrane amalgamation near the Median Tectonic Line. *N.Z. J. Geol. Geophys.*, 36, pp.117–125.
- Bradshaw, J.D., 1989. Cretaceous geotectonic patterns in the New Zealand region. *Tectonics* 8, pp.803–820.
- Brathwaite, R.L.; Pirajno, F., 1993. Metallogenic map of New Zealand. Lower Hutt: Institute of Geological & Nuclear Sciences. *Institute of Geological & Nuclear Sciences*, monograph, p.215.
- Burrows, D.R., Spooner, E.T.C., 1987. Generation of a magmatic H₂O-CO₂ fluid enriched in Au, Mo, and W within an Archean sodic granodiorite stock, Mink Lake, northwestern Ontario. *Econ. Geol.*, 82, pp.1931–1957.
- Christie, A.B.; Corner, N.G.; Bierlein, F.P.; Smith P.K., Ryan, R.J., A. & D.C., 2000. Disseminated gold at Reefton, South Island, New Zealand, compared with similar occurrences in Victoria, Australia and Nova Scotia, Canada. *NZ Mining*, 28, pp.25–33.
- Christie, A.B. & Brathwaite, R.L., 2003. Hydrothermal alteration in metasedimentary rock-hosted orogenic gold deposits, Reefton goldfield, South Island, New Zealand. *Mineralium Deposita*, 38(1), pp.87–

- Christie, A.B. & Brathwaite, R.L., 2002. Orogenic gold deposits in New Zealand: a new wall poster. , (1997), pp.351–357.
- Clark, R.H., Wellman, H.W., 1959. The Alpine Fault from lake McKerrow to Milford Sound. *N.Z. J. Geol. Geophys.*, 2, pp.590– 601.
- Coombs, D.S. et al., 1976. The Dun Mountain ophiolite belt, New Zealand, its tectonic setting, constitution, and origin, with special reference to the southern portion. *American Journal of Science*, 276(5), pp.561–603.
- Cooper, R.A., Tulloch, A.J., 1992. Early Paleozoic terranes in New Zealand and their relationship to the Lachlan Fold Belt. *Tectonophysics*, 214, pp.129–144.
- Cooper, R.A., 1974. Age of the Greenland and Waiuta Groups, South Island, New Zealand (Note). *New Zealand Journal of Geology and Geophysics*, 17(4), pp.955–962. Available at: <http://dx.doi.org/10.1080/00288306.1974.10418235>.
- Cox, S.F., 2005. Coupling between deformation, fluid pressures, and fluid flow in ore-producing hydrothermal systems at depth in the crust. *Economic Geology, 100th Anniversary Volume*, pp.39–75.
- Craw, D., Rattenbury, M.S. & Johnstone, R.D., 1987. Structural geology and vein mineralisation in the Callery River headwaters, Southern Alps, New Zealand. *New Zealand Journal of Geology and Geophysics*, 30(3), pp.273–286.
- Dean, W.E.J., 1974. Determination of carbonate and organic matter in calcareous sediments and sedimentary rocks by loss on ignition: Comparison with other methods. *Journal of Sedimentary Petrology*, 44(1), pp.242–248.
- Downey, J.F., 1928. *Quartz Reefs of the West Coast Mining District, New Zealand*, Cadsonbury Publications.
- Eilu, Pasi; Mikucki, Edward J; Groves, D.I., 1998. Wallrock alteration and primary geochemical dispersion in lode-gold exploration: notes from a short course presented at the Fourth Biennial Meeting of the Society for Geology Applied to Mineral Deposits (SGA) Turku, Finland, August 11-13, 1997. *Denver U. S. Geological Survey 1997*, SGA short , p.65.
- Eilu, P. & Mikucki, E.J., 1998. Alteration and primary geochemical dispersion associated with the Bulletin lode-gold deposit, Wiluna, Western Australia. *Journal of Geochemical Exploration*, 63(2), pp.73–103.
- Eilu, P., Mikucki, E.J. & Dugdale, A.L., 2001. Alteration zoning and primary geochemical dispersion at the Bronzewing lode-gold deposits, Western Australia. *Mineralium Deposita*, 36(1), pp.13–31.
- Fu, B., Fairmaid, a M. & Phillips, D., 2007. Gold Undercover. *Sciences-New York*, (September).
- Fyon, J.A., Troop, D.G., Marmont, S., & Macdonald, A.J., 1989. Introduction of gold into Archean crust, Superior Province, Ontario - Coupling between mantle-initiated magmatism and lower crustal thermal maturation. *Econ. Geol.*, Monograph, pp.479–490.
- Gao, Z.L. et al., 1995. Supergene ore and hypogene nonore mineralization at the Nagambie sediment-hosted gold deposit, Victoria, Australia. *Economic Geology*, 90(6), pp.1747–1763.
- GNS, S., 2012. Explore West Coast (NZ) Minerals. , p.60.
- Goldfarb, R.J., Miller, L.D., Leach, D.L., Snee, L.W., 1997. Gold deposits in metamorphic rocks of Alaska. *Economic Geology*, (Monograph 9), pp.151–190.
- Goldfarb, R.. et al., 1991. Southeastern Alaska: Constraints on the Origin of Hydrothermal Fluids. *Economic Geology*, 86, pp.66–80.
- Goldfarb, R.J., Groves, D.I. & Gardoll, S., 2001. Orogenic gold and geologic time: A global synthesis. *Ore Geology Reviews*, 18(1-2), pp.1–75.
- Goldfarb, R.J. & Miller, L.D., 1997. *Mineral deposits of Alaska* R. J. M. Goldfarb Lance D., ed., Economic Geology Publishing Company.
- Goldfarb, R.J. et al., 2005. Distribution , Character , and Genesis of Gold Deposits in Metamorphic

- Terranes. *Economic Geology 100th Anniversary Volume*, pp.407–450.
- Gorman, P.J., Kerrick, D.M. & Connolly, J.A.D., 2006. Modeling open system metamorphic decarbonation of subducting slabs. *Geochemistry, Geophysics, Geosystems*, 7(4).
- Graham, I.J., Mortimer, N., 1992. Terrane characterisation and timing of metamorphism in the Otago Schist, New Zealand, using Rb–Sr and K–Ar geochronology. *N.Z. J. Geol. Geophys*, 35, pp.391–401.
- Groves, D.I. et al., 2005. 100th Anniversary special paper: Secular changes in global tectonic processes and their influence on the temporal distribution of gold-bearing mineral deposits. *Economic Geology*, 100(2), pp.203–224.
- Groves, D.I. et al., 1998. Orogenic gold deposits: a proposed classification in the context of their crustal distribution and relationship to other gold deposit types. *Ore Geology Reviews*, 13(1-5), pp.7–27.
- Henderson, J., 1917. *The geology and mineral resources of the Reefton subdivision. Westport and North Westland divisions* W. M. F. Marks, ed., Government printer.
- Herron, M.M., 1988. Geochemical classification of terrigenous sands and shales from core or log data. *Journal of Sedimentary Research*, 58(5), pp.820–829.
- Herzer, R.H., 1995. Seismic stratigraphy of a buried volcanic arc, Northland, New Zealand and implications for Neogene subduction. *Mar. Pet. Geol*, 12, pp.551–561.
- Hodgson, C.J., Hamilton, J.V., 1989. Gold mineralization in the Abitibi greenstone belt: end-stage result of Archean collisional tectonics? *Econ. Geol.*, Monograph, pp.86–100.
- Hunt, P.A.; Roddick, J.C., 1993. A compilation of K–Ar and ⁴⁰Ar–³⁹Ar ages: report 23. In: Radiogenic age and isotope studies: report 7. *Geological Survey of Canada*, Pap 93-2, pp.127–154.
- Ishikawa, Yohei; Sawaguchi, T., Iwaya, S. & Horiuchi, M., 1976. Delineation of Prospecting Targets for Kuroko Deposits Based on. *Mining Geology*, 26(136), pp.105–117.
- Jowitt, S.M. et al., 2012. Quantifying the release of base metals from source rocks for volcanogenic massive sulfide deposits: Effects of protolith composition and alteration mineralogy. *Journal of Geochemical Exploration*, 118, pp.47–59.
- Kerrick, R., 1989. Lithophile element systematics of gold vein deposits in Archean greenstone belts: Implications for source processes. *Economic Geology*, (Monograph 6), pp.508–519.
- Kerrick, R., 2005. Metallogenic Provinces in an Evolving Geodynamic Framework. , pp.1097–1136.
- Kerrick, R. & Cassidy, K.F., 1994. Temporal relationships of lode gold mineralization to accretion, magmatism, metamorphism and deformation — Archean to present: A review. *Ore Geology Reviews*, 9(4), pp.263–310.
- Kimbrough, D.L., Mattinson, J.M., Coombs, D.S., Landis, C.A. & Johnston, M.R., 1992. Uranium–lead ages from the Dun Mountain ophiolite belt and Brook Street terrane, South Island, New Zealand. *Geol. Soc. Am. Bull.*, 104, pp.429–443.
- Kimbrough, D.L., Tulloch, A.J., Coombs, D.S., Landis, C.A. & Johnston, M.R., Mattinson, J.M., 1994. Uranium–lead zircon ages from the Median Tectonic Zone, New Zealand. *N.Z. J. Geol. Geophys.*, 37, pp.393–419.
- Kishida, A. & Kerrick, R., 1987. Hydrothermal alteration zoning and gold concentration at the Kerr-Addison Archean lode gold deposit, Kirkland Lake, Ontario (Canada). *Economic Geology*, 82(3), pp.649–690.
- Kontak, D.J. et al., 1990. Integrated model for Meguma Group lode gold deposits, Nova Scotia, Canada. *Geology*, 18 (3), pp.238–242. Available at: <http://geology.gsapubs.org/content/18/3/238.abstract>.
- Landis, C.A., Coombs, D.S., 1967. Metamorphic belts and orogenesis in southern New Zealand. *Tectonophysics* 4, pp.501–518.
- Large, R.R., Gemmell, J.B. & Paulick, H., 2001. The alteration box plot: A simple approach to understanding the relationship between alteration mineralogy and litho-geochemistry associated with volcanic-hosted massive sulfide deposits. *Economic Geology*, 96(5), pp.957–971.
- Leach, T; Corbett, G.J.; Magner, P.; McKenzie, M., 1997. A geological model for gold mineralisation at

- Reefton, New Zealand. Proceedings of the 1997. In *New Zealand minerals and mining conference, Crown Minerals, Ministry of Commerce*, pp. 159–165.
- Lew, J. H.; Corner, N.G., 1988. The Globe-Progress prospect, Reefton, New Zealand. In: Goode, A. D. T.; Smyth, E. L.; Birch, W. D.; Bosma, L. I. ed. Bicentennial gold 88. *Geological Society of Australia Abstracts*, Series 23, pp.271–273.
- MacKenzie, D.J. & Craw, D., 2007. Contrasting hydrothermal alteration mineralogy and geochemistry in the auriferous Rise & Shine Shear Zone, Otago, New Zealand. *New Zealand Journal of Geology and Geophysics*, 50(2), pp.67–79.
- MacKinnon, T.C., 1983, 1983. Origin of the Torlesse terrane and coeval rocks, South Island, New Zealand. *Geol. Soc. Am. Bull*, 94, pp.967–985.
- Maw, L., 2001. Greenland Group deformation and the structural controls of gold mineralisation within the Reefton goldfield: from the General Gordon to the Golden Lead. In *Proceedings of the 34th Annual Conference of the New Zealand Branch of the Australasian Institute of Mining and Metallurgy*. pp. 215– 226.
- Moritz, R., 2000. *What Have We Learnt About Orogenic Lode Gold Deposits Over The Past 20 Years?*, University of Geneva, Switzerland.
- Mortimer, N., Tulloch, A., 1996. The Mesozoic basement of New Zealand. Mesozoic Geology of the Eastern Australian Plate Conference (Abstr.). *Geol. Soc. Aust.*, 43, pp.391–399.
- Mortimer, N., 1995. Origin of the Torlesse Terrane and coeval rocks, North Island, New Zealand. *Int. Geol. Rev.*, 36, pp.891– 910.
- Muir, R.J. et al., 1994. Ion microprobe U-Pb zircon geochronology of granitic magmatism in the Western Province of the South Island, New Zealand. *Chemical Geology*, 113(1-2), pp.171–189.
- Nathan, S., 1976. Geochemistry of the Greenland Group (early Ordovician), New Zealand. *New Zealand Journal of Geology and Geophysics*, 19(5), pp.683–706.
- Nathan, S., 1978. Geological map of New Zealand 1:63,360 Sheet S44 Greymouth. 1st ed. Wellington: Department of Scientific and Industrial Research. *Geological map of New Zealand 1:63,360 S44. 1 fold. map + 1 booklet*.
- Nesbitt, B.E., Murowchick, J.B. & Muehlenbachs, K., 1986. Dual origins of lode gold deposits in the Canadian Cordillera. *Geology*, 14(6), pp.506–509.
- Phillips, G.N. & Powell, R., 2010. Formation of gold deposits: A metamorphic devolatilization model. *Journal of Metamorphic Geology*, 28(6), pp.689–718.
- Phillips, G.N. & Powell, R., 1993. Link between gold provinces. *Economic Geology*, 88(5), pp.1084–1098.
- Pitcairn, I.K., Warwick, P.E., et al., 2006. Method for ultra-low-level analysis of gold in rocks. *Analytical Chemistry*, 78(4), pp.1290–1295.
- Pitcairn, I.K., Teagle, D. a H., et al., 2006. Sources of metals and fluids in orogenic gold deposits: Insights from the Otago and Alpine schists, New Zealand. *Economic Geology*, 101(8), pp.1525–1546.
- Price, G., 2015. Gold price trends 1973 to 2015. Available at: <http://www.goldprice.org/> [Accessed January 12, 2016].
- Ramsay, J.G., 1980. The crack-seal mechanism of rock deformation. *Nature*, 284(5752), pp.135–139.
- Ramsay, W.R.H. et al., 1998. Turbidite-hosted gold deposits of central Victoria, Australia: their regional setting, mineralising styles, and some genetic constraints. *Ore Geology Reviews*, 13(1-5), pp.131–151.
- Rattenbury, M.S. & Stewart, M., 2000. Structural setting of the Globe-Progress and Blackwater gold mines, Reefton goldfield, New Zealand. *New Zealand Journal of Geology and Geophysics*, 43(3), pp.435–445.
- Ridley, J.R. & Diamond, L.W., 2000. Fluid chemistry of orogenic lode gold deposits and implications for genetic models. *Reviews in Economic Geology*, 13, pp.141–162.
- Rock, N.M.S., Groves, D.I., Perring, C.S., Golding, S.D., 1989. Gold, lamprophyres, and porphyries: what does their association mean? *Economic Geology*, (Monograph 6), pp.609–625.

- De Ronde, C.E.J. et al., 2000. Round Hill shear zone-hosted gold deposit, Macraes Flat, Otago, New Zealand: Evidence of a magmatic ore fluid. *Economic Geology*, 95(5), pp.1025–1048.
- Roser, B.P., Mortimer, N., Turnbull, I.M., Landis, C.A., 1993. Geology and geochemistry of the Caples terrane, Otago, New Zealand: compositional variations near a Permo-Triassic arc margin. In: Ballance, P.F. (Ed.), *South Pacific Sedimentary Basins. Sedimentary Basins of the World 2, Elsevier, Amsterdam*, pp.3–19.
- Roser, B.P. et al., 1996. Reconnaissance sandstone geochemistry, provenance, and tectonic setting of the lower Paleozoic terranes of the West Coast and Nelson, New Zealand. *New Zealand Journal of Geology and Geophysics*, 39(1), pp.1–16.
- Roser, B.P. & Nathan, S., 1997. An evaluation of elemental mobility during metamorphism of a turbidite sequence (Greenland Group, New Zealand). *Geological Magazine*, 134(02), pp.219–234.
- Saunders, J. a. et al., 2013. *Geochemistry of Hydrothermal Gold Deposits*, Available at:
- Sibson, R.H., Robert, F. & Poulsen, K.H., 1988. High-Angle Reverse Faults, Fluid-Pressure Cycling, and Mesothermal Gold-Quartz Deposits. *Geology*, 16(6), pp.551–555.
- Skinner, D.N.B. & Brathwaite, R.L., 1999. Mesozoic mesothermal quartz-gold-scheelite lodes, Wakamarina, Marlborough, New Zealand. *New Zealand Journal of Geology and Geophysics*, 42(November 2013), pp.335–348.
- SNL Metals Economics Group, 2013. Worldwide Exploration Worldwide Exploration Trends. *Metals Economics Group*, (PDAC International Convention 2010), pp.1–8.
- Stüwe, K., 1998. Tectonic constraints on the timing relationships of metamorphism, fluid production and gold-bearing quartz vein emplacement. *Ore Geology Reviews*, 13(1-5), pp.219–228.
- Sutherland, R., 1999. Basement geology and tectonic development of the greater New Zealand region: An interpretation from regional magnetic data. *Tectonophysics*, 308(3), pp.341–362.
- Sutherland, R., 1995. The Australia–Pacific boundary and Cenozoic plate motions in the southwest Pacific: some constraints from GEOSAT data. *Tectonics*, 14, pp.819–831.
- Sutherland, R., Davey, F. & Beavan, J., 2000. Plate boundary deformation in South Island, New Zealand, is related to inherited lithospheric structure. *Earth and Planetary Science Letters*, 177(3-4), pp.141–151.
- Teagle, D.A.H., Norris, R.J. and Craw, D., 1990. Structural controls on gold-bearing quartz mineralisation in a duplex thrust system, Hyde-Macraes shear zone, Otago Schist, New Zealand. *Economic Geology*, 85, pp.1711–1719.
- Tenthorey, E. & Cox, S.F., 2003. Reaction-enhanced permeability during serpentinite dehydration. *Geology*, 31(10), pp.921–924.
- Tulloch, A.J., 1988. Batholiths, plutons, and suites: nomenclature for granitoid rocks of Westland-Nelson, New Zealand. *N.Z. J. Geol. Geophys.*, 30, pp.505–509.
- Tulloch, A.J., 1983a. Granitoid rocks of New Zealand – a brief review. *Geological Society of America*, 159, pp.5–20.
- Tulloch, A.J., 1983b. Granitoid rocks of New Zealand—a brief review. *Geological Society of America Memoirs*.
- Vielreicher, N.M., Ridley, J.R. & Groves, D.I., 2002. Marymia: an Archean, amphibolite facies-hosted, orogenic lode-gold deposit overprinted by Palaeoproterozoic orogenesis and base metal mineralisation, Western Australia. *Mineralium Deposita*, 37(8), pp.737–764.
- Williams, G.J., 1974a. Economic geology of New Zealand. *Australasian Institute of Mining and Metallurgy*, Monograph .
- Williams, G.J., 1974b. *Economic Geology of New Zealand*, Australian Institute of Mining and Metallurgy, Monograph Series 4.
- Zhu, Y., An, F. & Tan, J., 2011. Geochemistry of hydrothermal gold deposits: A review. *Geoscience Frontiers*, 2(3), pp.367–374.

Acknowledgements

I would like to thank my supervisors Dr. Iain Pitcairn (Stockholm University) and Professor Dave Craw (University of Otago) for their advice and the knowledge they shared during the completion of this thesis project. It has been a steep learning curve and I am immensely grateful for your patience. I would also like to thank Oceana Gold Corporation and its staff in Reefton for making this project possible by giving access to the core and their facilities in Reefton as well as providing accommodation during the fieldwork. University of Otago through Professor Dave Craw provided logistical support and I am thankful for that. This thesis has been produced during the period I obtained my scholarship provided by the Swedish Institute at Stockholm University, thanks to The Swedish Institute scholarship programme.

I am grateful to Dan Zetterberg, Arman Boskabadi, Cora Wohlgemuth-Ueberwasser and Runa Jacobsson for helping out with the lab work and I am also thanking Clifford Patten for his assistance during data analysis.

I would also like to thank the academic, administrative and technical staff in the Department of Geological Sciences at Stockholm University for the hard work accomplished to provide an education of quality for the master's programme. I would like to thank all my colleagues and friends and all the people met during my studies, it has been an amazing 2 years on this campus that I will surely miss you all.

I would like to give a special thanks to my parents and family for always believing in me and literally driving forces in my life.

And last but not least, Michaela Hubmann, you have been present since day 0 when I embarked on this journey; poor you, you got to read all my "undecipherable" essays and watch all the geology documentaries with me, thanks a lot to you, you are "rocking" my life.